Matter

Article

Closed-loop optimization using machine learning for the accelerated design of sustainable cements incorporating algal biomatter

Graphical abstract

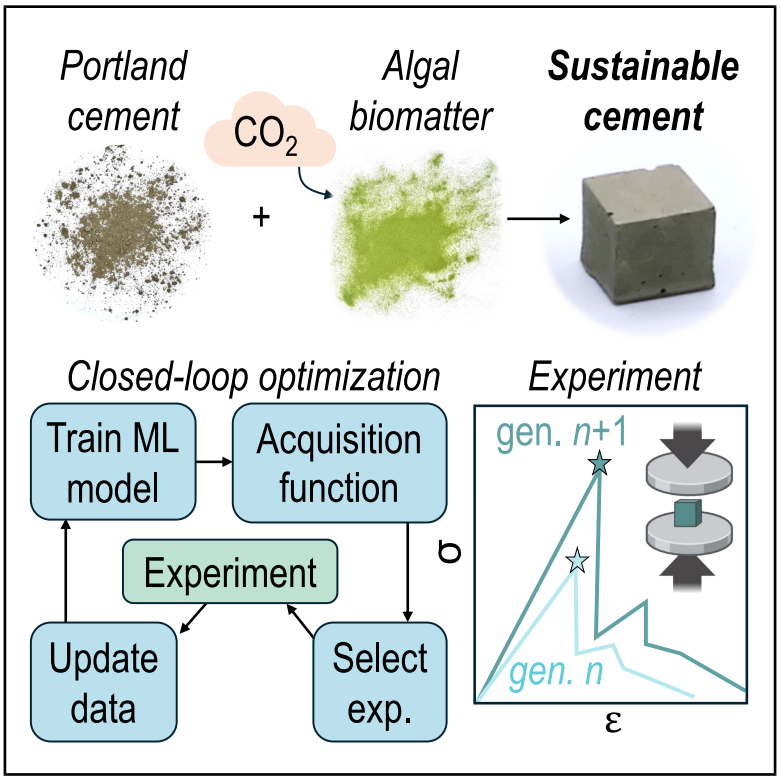

Highlights

- ML-guided experimental framework enables closed-loop optimization of new materials
- New algae cement is optimized to improve GWP while keeping functional strength
- Amortized Gaussian process model with early stopping accelerates optimization process
- Model-informed knowledge provides understanding of modified cement hydration

Authors

Meng-Yen Lin, Kristen Severson, Paul Grandgeorge, Eleftheria Roumeli

Correspondence

kseverson@microsoft.com (K.S.), eroumeli@uw.edu (E.R.)

In brief

Reducing cement's carbon footprint is crucial to mitigating greenhouse gas emissions. However, developing novel, low-impact alternatives remains time and resource intensive. Here, we present a machine-learning-guided, closed-loop experimental framework for the accelerated optimization of new algae-based cements. This approach integrates life-cycle assessments into real-time experimentation, reducing environmental impact while meeting structural strength requirements and providing scientific insights into cement hydration. The design framework demonstrates the potential to expedite the development of novel sustainable materials with high performance.

Benchmark
First qualification/assessment of material properties and/or performance

Lin et al., 2025, Matter 8, 102267
September 3, 2025
Published by Elsevier Inc.
https://doi.org/10.1016/j.matt.2025.102267

CellPress

Matter

CellPress
OPEN ACCESS

Article

Closed-loop optimization using machine learning for the accelerated design of sustainable cements incorporating algal biomatter

Meng-Yen Lin,[1,3] Kristen Severson,[2,3,*] Paul Grandgeorge,[1] and Eleftheria Roumeli[1,4,*]
[1]Department of Materials Science and Engineering, University of Washington, Seattle, WA 98195, USA
[2]Microsoft Research, Cambridge, MA 02139, USA
[3]These authors contributed equally
[4]Lead contact
*Correspondence: kseverson@microsoft.com (K.S.), eroumeli@uw.edu (E.R.)
https://doi.org/10.1016/j.matt.2025.102267

PROGRESS AND POTENTIAL The concrete industry is a large producer of global greenhouse gases, the majority of which are attributable to ordinary Portland cement. Our research demonstrates a sustainable alternative by incorporating whole macroalgae as a biomatter substitute in cement. Biomatter is a natural choice for meeting sustainability goals, but it introduces complexity in the material design. Using machine learning and a life-cycle assessment (LCA)-integrated design, we significantly accelerated the discovery of an algal cement formulation that reduces global warming potential by 21% while still meeting strength requirements. The long-term vision of this research is to serve as a foundation for the accelerated design of sustainable biomaterials. The progress presented here not only offers a tangible step toward lowering the carbon footprint of cement but also provides a proof point of the utility of a framework for materials design that integrates LCA with experimental testing and computational modeling.

SUMMARY

The substantial embodied carbon of cement, coupled with the ever-increasing need for construction materials, motivates the need for more sustainable cementitious materials. An emerging strategy to mitigate CO_2 emissions involves incorporating carbon-negative biomatter; however, this introduces new challenges due to complex hydration-strength relationships and the combinatorial design space. Here, using machine learning, we develop a closed-loop optimization strategy to accelerate green-cement design with minimal CO_2 emissions while meeting compressive-strength criterion. Green cements incorporating algae are tested in real time to predict strength evolution, with early-stopping criteria applied to accelerate the optimization process. This approach, using only 28 days of experiment time, attains both the strength requirement and 93% of the achievable improvement in global warming potential (GWP), resulting in a cement that has a 21% reduction in GWP. We further validate model-informed relationships via analysis of hydration, demonstrating the potential for developing materials grounded in scientific understanding.

INTRODUCTION

To meet the goal of reducing global greenhouse gas (GHG) emissions by 45% by 2030 and achieve net zero by 2050,[1] urgent actions are required. To that end, the concrete industry, responsible for 8%–11% of global CO_2 emissions,[2,3] is under significant pressure to reduce its carbon footprint. Cement production, which contributes 90% of the carbon emissions of concrete,[4] is a key target. Strategies to mitigate its GHG emissions include the use of alternative fuels[5,6] or decreasing the amount of cement in the cementitious binder. For the latter, research has focused on incorporating industrial wastes, such as fly ash,[7] granulated blast furnace slag,[8] or silica fume,[9] as supplementary cementitious materials (SCMs) or forming alkali-activated cement-free geopolymers.[10] However, sourcing SCMs from carbon-intensive industries and the chemical treatments required may not be sufficient to meet GHG goals.[11]

A promising alternative for sustainable materials involves using fast-growing, untreated plant, algal, or microbial biological matter (biomatter) as polymeric matrices or fillers.[12–16] Among these, algal biomatter stands out due to its combined carbon-negative potential, rapid growth on non-arable land, and

Please cite this article in press as: Lin et al., Closed-loop optimization using machine learning for the accelerated design of sustainable cements incorporating algal biomatter, Matter (2025), https://doi.org/10.1016/j.matt.2025.102267

availability. Although the properties of these biomaterials suggest they could significantly mitigate the carbon footprint of cementitious materials, the concept of utilizing intact algal biomatter in the design of green-cement formulations remains largely unexplored. Recent studies[17–19] found that microalgae can retard cement hydration without compromising strength at concentrations below c = 5 wt % but completely hinder hydration reactions, leading to final strength reductions of more than 85%, at higher concentrations.[18] Improving understanding of the interactions between algae and cement and their impact on strength is critical to developing sustainable cement for construction.

Designing novel biomatter cements is challenging due to the complexity of materials and combinatorial design space. Traditional trial-and-error approaches are inefficient, especially as 28-day compressive strength is the standard target property, introducing delays in the design cycle. Design of experimental approaches aims to reduce the number of experiments via the use of surrogate input-output models.[20,21] Recent advancements in machine learning (ML) have improved predictive capabilities in concrete science,[22,23] but ML models typically require large datasets to learn the relevant relationships. To address this, some studies have incorporated domain knowledge, enabling improved predictive performance with fewer samples. For instance, Li et al.[24] incorporated properties derived from empirical and physical models into the training datasets and demonstrated improved training convergence, performance with small datasets, extrapolation capability from laboratory to on-site data, and robustness to outliers. Pfeiffer et al.[25] and Ament et al.[26] developed Gaussian process models for time-evolving concrete properties, but these still rely on 28-day compressive-strength data.

In this study, we demonstrate a closed-loop experimental design framework for accelerating the discovery of sustainable green-cement formulations. Specifically, we aim to discover the formulation with the minimum global warming potential (GWP) while meeting a 28-day compressive-strength criterion. We address several shortcomings of past approaches. First, we introduce a novel material system by incorporating the green macroalgae, *Ulva* spp. (hereinafter *Ulva*), to partially replace ordinary Portland cement (OPC). *Ulva* was selected not only due to its local availability and established use in other sustainable materials research[27] but also because we hypothesized that its tissue and hierarchical structure may provide better structural reinforcement and fewer hindrance effects to cement hydration compared to microalgae. Furthermore, it would serve as a carbon sink. The application of intact macroalgae, and *Ulva* in particular, to the best of our knowledge has not been explored to date. In contrast to studies applying ML to cementitious systems with conventional SCM relying on existing databases,[22,28] our proposed material system serves as an example of how new algae cements can be developed, highlighting both the challenges and potential of this promising material class. We introduce a domain-knowledge-informed ML model capable of high predictive performance with a small number of samples, thereby circumventing the time- and resource-intensive data-curation process that has challenged past studies. In addition, inspired by early-stopping methods in ML training,[29–32] we introduce a novel early-stopping criteria to terminate experiments prior to 28 days. We compare the optimization efficiency of this approach with other conventional models, showing an accelerated design process without sacrificing performance. Finally, we validate the interpretability of our approach with materials characterization to verify the relationships learned by the ML model. By proactively utilizing GWP to inform the optimization of real-time experimentation—rather than conducting multi-objective optimization *post hoc*[25,33]—this work establishes a framework with the potential to accelerate the design of sustainable cement with feasible experimental resources while satisfying critical performance requirements.

RESULTS

Designing an efficient methodology for the discovery of environmentally friendly cement

Our goal is to accelerate the design of a novel green-cement formulation, which meets a specified strength criterion while minimizing GWP. In this section, we describe the four primary components of our design approach: the design space, the estimation of GWP, the prediction of compressive strength, and the design of experiments with early termination. A summary of our approach can be found in Figure 1.

Design space

We select 28-day compressive strength as the design property of interest as this is often used as the minimum specification for green cements. Based on American Society for Testing and Materials (ASTM)standard C150,[34] we specifically set the 28-day compressive-strength target to 28 MPa plus a safety factor of 10%, resulting in a final minimum strength criterion of 30.8 MPa. Motivated by optimizing factors that likely impact compressive strength, we select the design space of *Ulva* concentration (c, in g of *Ulva*/g of solid powder), *Ulva* average particle size (*APS*, in μm), water-cement ratio (wc, in g of water/g of OPC), and environmental humidity (*RH*) during the initial 7-day curing process (see Figure 1A). For each variable of the design space, we specify an upper and lower bound and an interval size to define the search space. Based on the drastic strength reduction at high biomatter concentration shown in previous microalgae-cement studies,[17,18] we scan the *Ulva* concentration up to 15 wt % with the interval of 0.5 wt %. Meanwhile, we consider water-cement ratios from 0.38 to 0.5 as typically recommended for cementitious materials with varying filler sizes to ensure full hydration.[35] Using blade milling, ball milling, and sieving, *Ulva* particle sizes are divided into four classes, and the humidity of the curing environment is set in three levels representing low, medium, and high relative humidity (see Table 1 for a summary).

Global warming potential

A life-cycle assessment (LCA) is conducted to quantify the environmental impact of the green cement in order to compare the environmental benefits with commercial Type I/II Portland cement. In this case study, the GWP is selected as an index of the environmental impact due to the stress on the high carbon footprint generated by the cement production processes and is calculated based on attributional LCA.[36] Aiming to accelerate the design process of green cement, the scope of this study is presumed to be at the laboratory scale rather than the industrial

Please cite this article in press as: Lin et al., Closed-loop optimization using machine learning for the accelerated design of sustainable cements incorporating algal biomatter, Matter (2025), https://doi.org/10.1016/j.matt.2025.102267

CellPress
OPEN ACCESS

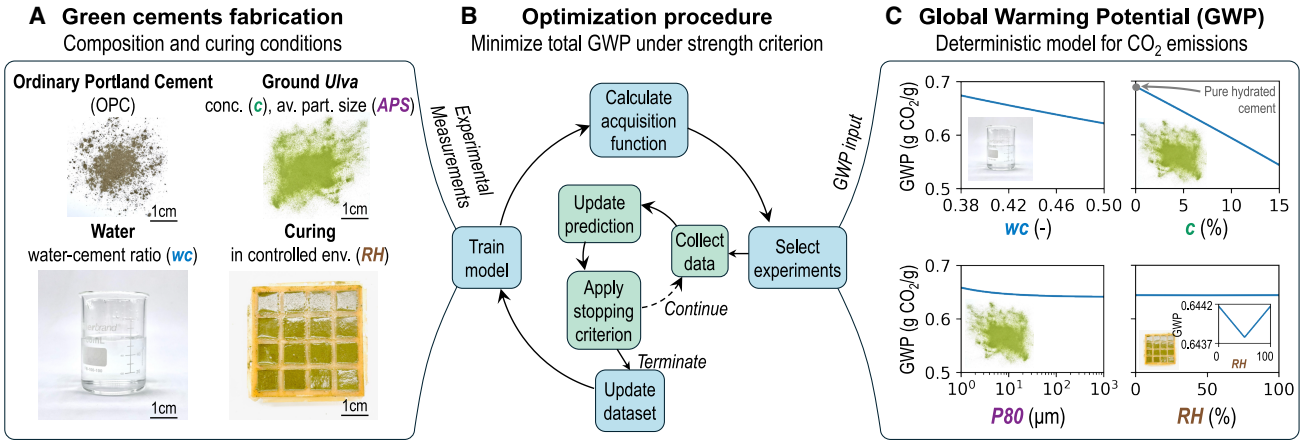

Figure 1. Closed-loop optimal experimental design for accelerating the discovery of green cement

(A) Composition and conditions of the fabrication of *Ulva* cements. Ordinary Portland cement (OPC) is mixed with ground *Ulva* and water before casting in cubic rubber molds and curing in an environment of controlled humidity.

(B) Optimization procedure is built on two loops. The *outer* loop (blue) selects formulations from the design space to be tested based on the associated GWP and predicted strength values. The *inner* loop (green) determines whether an experiment should continue.

(C) Variation of the global warming potential (GWP, reported in g CO_2/g hydrated green cement) as a function of the four design parameters (*wc*, *c*, *P*80, and *RH*). In each plot, one parameter is varied while the other three are fixed using the following default values: *wc* = 0.45, *c* = 5%, *APS* = 37.40 μm (corresponding to *P*80 = 98.7 μm), and *RH* = 50%.

scale. To focus on the impact of the formulation and processing of green cement, other factors involving the locations and transportation of the raw materials and products are excluded, resulting in a system boundary only including the cultivation of *Ulva*, collection of Portland cement, and the manufacturing processes including humidity-controlled curing for 7 days. The system boundary and the process flow diagram are shown in Figure S1. The declared unit of the final product is defined to be 1 g of hardened green cement after 28 days of curing.

The GWP, expressed in grams of CO_2 emitted per gram of hydrated *Ulva* cement, was estimated using a deterministic model relying on relevant values for specific CO_2 emissions from the literature. GWP is assumed to be a function only of the four parameters of our design space: water-cement ratio, *Ulva* concentration, *Ulva* particle size, and relative humidity during the first 7 days of hydration, as described in the preceding section. Note that, within this deterministic CO_2 assessment, the particle size is represented by *P*80 (see Figure S2) since this attribute is generally used to assess the energy input necessary to reduce particle size using the Bond work index.[37] Throughout the rest of the manuscript, however, the particle size is characterized by the *APS*, providing a more intuitive size than *P*80. Additionally, relative humidity influences only the curing process rather than the material compositions, making it an independent parameter for a separate GWP calculation. The GWP is calculated using the following relation:

$$GWP = \frac{\mu_{OPC} + \frac{c}{1-c}\cdot\mu_{Ulva}(P80) + wc\cdot\mu_{water}}{1 + wc + \frac{c}{1-c}} + \mu_{RH}(RH), \quad \text{(Equation 1)}$$

where the symbol μ corresponds to specific CO_2 emissions for each component or curing condition associated with the green-cement fabrication.

To provide a reasonable optimization framework, our model is based on typical values of specific CO_2 emissions from literature and some simplifying assumptions enabling a comprehensive model. It should, however, be noted that, in practical industrial settings, the specific CO_2 emissions can vary widely and the values used in our model are therefore not universally accurate. Still, the general framework presented can be adapted using other values of specific CO_2 emissions. The most important aspect of our GWP expression is that it contains terms of positive emissions (e.g., $\mu_{OPC} > 0$) and negative emissions (e.g., $\mu_{Ulva} < 0$), corresponding to carbon sequestration during growth of the *Ulva* through photosynthesis. In this model, we assume that CO_2 absorption is permanent, i.e., no CO_2 emission will occur from the incorporation of *Ulva* in the green cements during the curing process, based on the measurement of CO_2 emission described in Note S1. The value and the variation of each emission term of Equation 1 are described in detail in the "attributional LCA: Deterministic model for specific CO_2 emissions" section and a summary is provided in Figure 1C.

Table 1. Definition of the design space

Parameter	Symbol	Unit	Values
Ulva concentration	*c*	wt % ($100 \times g_{ulva}/(g_{ulva} + g_{an.c})$)	[0.5, …, 14.5, 15.0]
Water-cement ratio	*wc*	[-] ($g_{water}/g_{an.c}$)	[0.38, …, 0.48, 0.50]
Average particle size	*APS*	μm	[2.86, 37.40, 138.49, 388.27]
Relative humidity	*RH*	%	[10, 50, 95]

Please cite this article in press as: Lin et al., Closed-loop optimization using machine learning for the accelerated design of sustainable cements incorporating algal biomatter, Matter (2025), https://doi.org/10.1016/j.matt.2025.102267

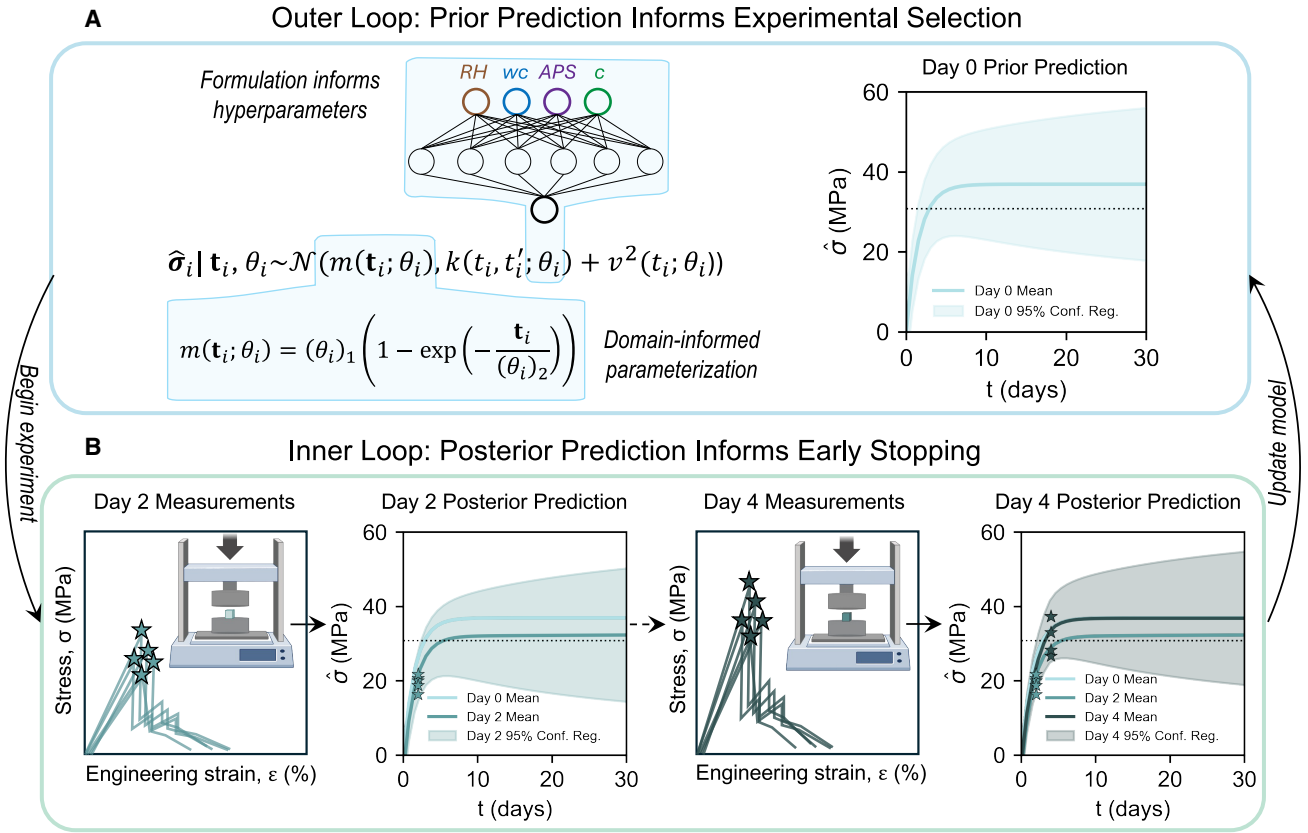

Figure 2. An example of the application of the aGP model for strength prediction during closed-loop testing for accelerated design

(A) The outer loop selects experimental formulations based on a criterion that considers both the GWP and the prediction of 28-day compressive strength.

(B) The inner loop uses the sequentially measured experimental data to update the compressive-strength prediction of the suggested formulation. If the predicted strength meets the termination criteria, no further data are collected for the formulation. If it fails to meet the termination criteria, data collection continues to the next time point. At the end of the round, all experimental data are used to update the aGP model and the process is repeated.

Predictive model

To predict the compressive strength based on the design space features of cementitious materials, we selected a class of models to meet the following aims: (1) incorporation of domain knowledge to enable learning from a small number of samples, (2) uncertainty quantification to enable Bayesian optimization, and (3) predictions that adapt to early strength measurements. To achieve all three aims, we leverage an amortized Gaussian process (aGP) model,[25] a class of Gaussian process (GP) model that employs a hyperparameter network to predict the required GP hyperparameters. An aGP models each element of the design space using its own GP model. As a GP specifies a distribution, uncertainty quantification (aim 2) is natively addressed. Since aGP models are most effective when defined with a non-zero mean function, we introduce a domain-inspired mean function based on the exponential function proposed for the strength evolution of algae-based cements[18]

$$\sigma = \sigma_f\left(1 - \exp\left(-\frac{t}{\tau}\right)\right), \qquad \text{(Equation 2)}$$

where σ is the compressive strength, σ_f is the final strength, t is time, and τ is the characteristic time. The parameters σ_f and τ are modeled as hyperparameters and are predicted by the hyperparameter network. The formulation introduces a strong prior and addresses aim 1 (see Figure 2A). Finally, we employ the ability of GP models to condition on data to allow for updated predictions based on early measurements (aim 3; see Figure 2B). This approach contrasts with more standard approaches aiming to predict only the design property of interest, i.e., 28-day compressive strength. See the "prediction of compressive strength" section for additional methodological detail.

Accelerated optimization

Our experimentation proceeds in rounds, each composed of an outer and inner loop component. To efficiently search the design space, during the outer loop, used to select which formulations to test, we prioritize experiments based on their ability to improve upon the current best GWP and their likelihood of meeting the strength criterion (Figure 2A). Once a formulation is selected, it proceeds to the inner loop (Figure 2B). At each time point, compressive strength is measured and the early-stopping criterion is applied to determine if experimentation should continue or terminate, using the posterior prediction to make this determination. An example of the application of the inner and outer loop criteria can be found in Figure 2. The

Please cite this article in press as: Lin et al., Closed-loop optimization using machine learning for the accelerated design of sustainable cements incorporating algal biomatter, Matter (2025), https://doi.org/10.1016/j.matt.2025.102267

CellPress
OPEN ACCESS

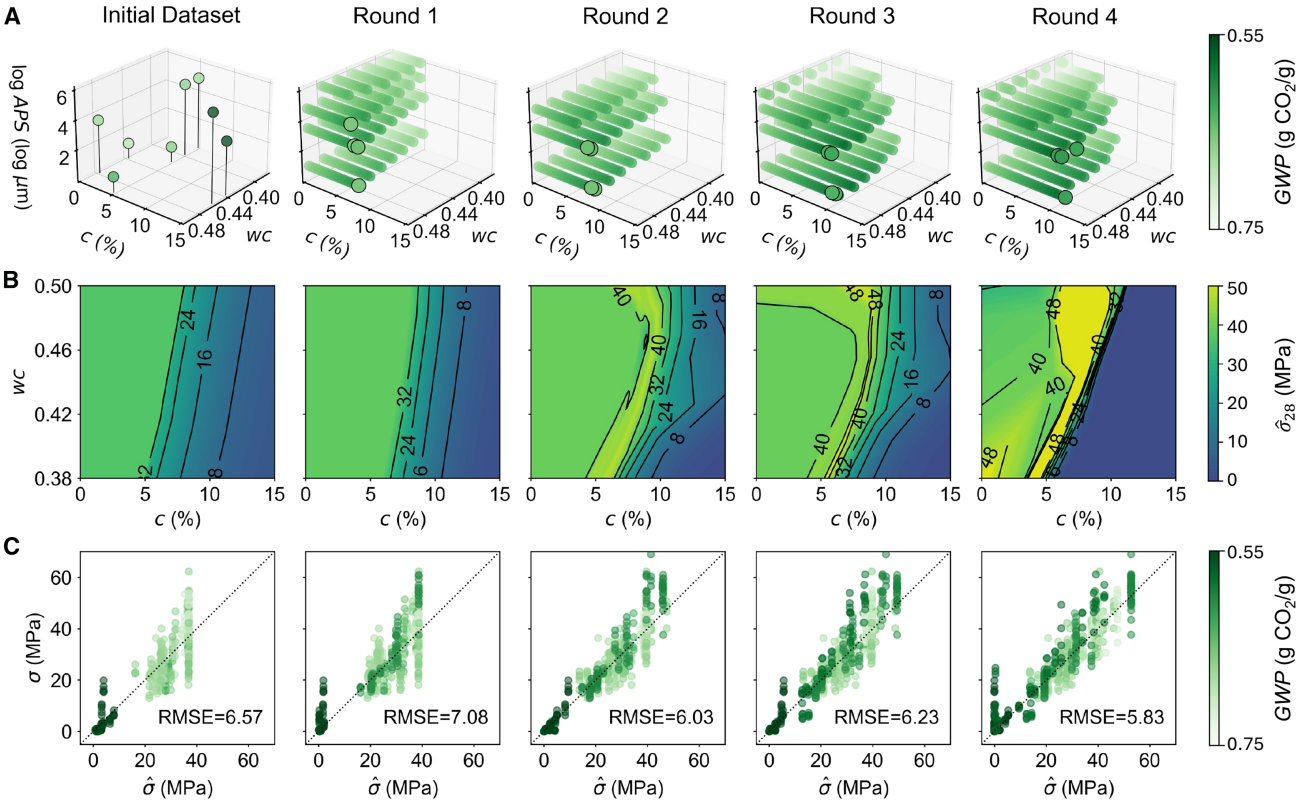

Figure 3. An overview of model evolution during accelerated design

(A) The initial dataset shows the data that were collected during initial experimentation based on LHS and its corresponding GWP. The subsequent plots from rounds 1 to 4 depict the strength-qualifying formulations at the outset of each round, which evolves non-linearly as the predictive model is updated with new data. The selected formulations of the minimal GWP for testing in the next round are also shown in each plot, as noted with black circles. All plots only show data at 95% RH.

(B) Contour plots indicate the predicted 28-day compressive strength $\hat{\sigma}_{28}$ as a function of water-cement ratio *wc* and *Ulva* concentration *c*. All plots show data at 95% RH and 37.4μm *APS*. In combination with (A), we observe the frontier of qualifying formulations shifting to higher concentrations of biomatter.

(C) The retrospectively observed performance of the predictive model at each round, comparing the estimated compressive strength $\hat{\sigma}$ and measured compressive strength σ at different time points. Note that this characterization of model performance is based on predictions of 28-day compressive strength that are made prior to observation of compressive strength on day 28.

"accelerated optimization algorithm" section contains further methodological detail.

Quantification and comparison of accelerated design process

Assessing the closed-loop optimization

To evaluate the optimization process and the efficiency of our experimental design, here we demonstrate the results of the sequential training from four rounds of closed-loop optimization. Given a budget of 28 days, corresponding to four rounds of experimentation time, and the initial aGP model trained an initial dataset of 24 formulations (see the "design space and initial data collection" section for detail), we began closed-loop testing. Based on the observed data, the initial best GWP was 0.626 g CO_2/g. The recommended formulations for the first round of optimization (as shown in Figure 3A; Table S1) focus on 95% *RH*, *wc* = 0.5, *Ulva* concentration *c* in the range of 7–8%, and *APS* less than 388.27 μm. We conducted the real-time experiments according to the recommended formulations by the model and updated the day 2 compressive strength in the model. The formulation of *wc* = 0.5, *c* = 7%, *APS* = 37.4 μm, *RH* = 95% met the early-stopping criteria and was terminated as an accepted formulation. In contrast, the difference between the estimated and observed 2-day strength for the remaining three samples was sufficiently large to motivate continuing the experiment. After the updates from the experimental data on day 4, the model suggested only conducting a day 7 compression test on formulation *wc* = 0.5, *c* = 7%, *APS* = 138.49 μm, *RH* = 95% as the predictive strength may not be able to satisfy the requirement, and indeed, after day 7 testing, this formulation was rejected. At this point, all observed data were used to update the aGP model by fine-tuning the hyperparameter network. This process was repeated for rounds (weeks) 2–4, and all the explored formulations are shown in Figure 3A and Table S1. The majority (11 out of 16) of experiments were terminated based on day 2 measurements, with an average duration of 2.8 days. Only one experiment in the first round continued for 7 days. In the final round (week 4), the model reached a point where it suggested

Please cite this article in press as: Lin et al., Closed-loop optimization using machine learning for the accelerated design of sustainable cements incorporating algal biomatter, Matter (2025), https://doi.org/10.1016/j.matt.2025.102267

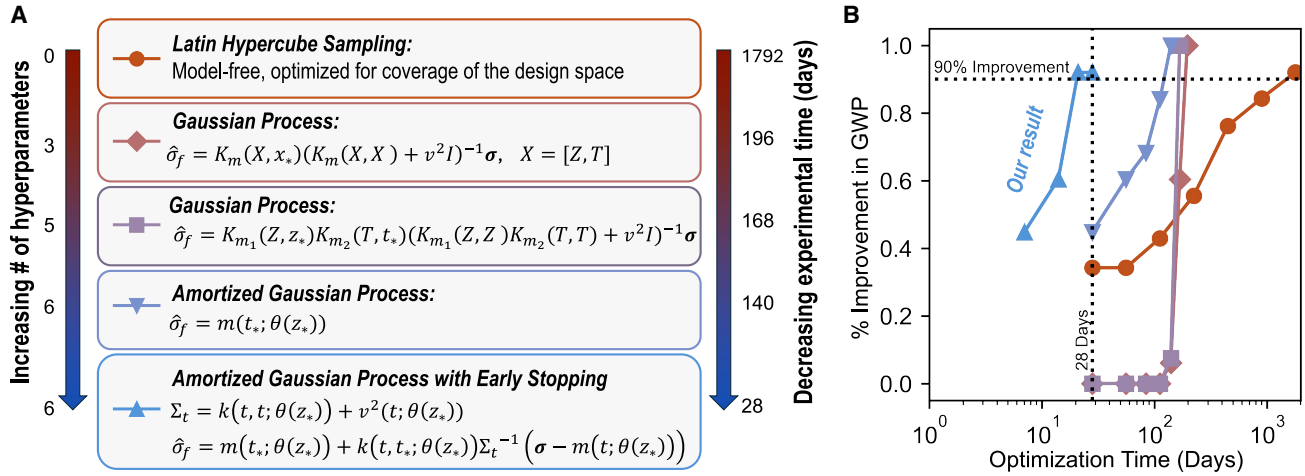

Figure 4. Comparison of optimization time to ≥90% improvement in GWP

(A) A summary of the five approaches considered for experimental design.

(B) Percentage of improvement in GWP as a function of experiment time for the five approaches.

formulations based on the best probability of improvement as there were no formulations predicted to qualify and improve on the current best GWP. At the end of four rounds, we proposed that *wc* = 0.5, *c* = 10.5%, *APS* = 37.4 μm, *RH* = 95% is the optimal formulation, with a GWP of 0.571 g CO_2/g, corresponding to a decrease of 0.055 g CO_2/g from the initial best GWP.

To validate our approach at the end of optimization, we measured the 28-day strength for all tested formulations. It was discovered that *wc* = 0.5, *c* = 11%, *APS* = 37.4 μm, *RH* = 95% is the true optimal, with a GWP of 0.567 g CO_2/g, indicating a maximum achievable GWP reduction of 0.059 g CO_2/g. During closed-loop testing, this formulation was erroneously predicted as non-qualifying; all other formulations (15 out of 16) were correctly categorized as meeting or not meeting the strength criterion. This means our approach resulted in 93% of the achievable decrease in GWP using only 28 days of experiment time. Overall, compared to a standard cement, assuming *c* = 0%, *RH* = 95%, and *wc* = 0.38, our suggested formulation leads to 21% reduction in GWP, from 0.725 to 0.571 g CO_2/g.

As the concentration of *Ulva* has the largest impact of our design space variables on GWP, we generally expected the optimization to prioritize maximizing the concentration. We see this manifest in the increasing *Ulva* concentration of formulations selected in each subsequent round (see Figure 3A). Interrogating our predictive model, we observe rapid evolution of the model's understanding of the relationship between *Ulva* concentration, water-cement ratio, and 28-day compressive strength as shown in Figure 3B. With the initial dataset, the model is able to identify that higher *Ulva* concentration requires a higher water-cement ratio and prioritizes this region. From round 1 to 4, the positive slope of *wc* vs. *c* gradually shifted to the right, where the recommended biomatter content increased from 7.5% to 11.5% while mostly focusing on higher *wc* from 0.48 to 0.5. Similarly, the model rapidly identifies lower *APS* as resulting in higher compressive strength, appropriately trading off the small increase in GWP due to lower *APS* for the possibility of increasing concentration (see Figure S3).

Retrospective analysis leveraging the 28-day compressive-strength measurements reveals the success of the aGP model. The improvement in prediction, as quantified in Figure 3C, despite using only strength data from an early age, is due to constraints imposed by the domain-informed mean function, which couples early and late strength measurements.

Comparing different experiment design strategies

As further validation of our approach in accelerated design, we consider four alternative experiment design methods and simulate the suggested formulations using an aGP model trained on all of the measured data collected after closed-loop experimentation, i.e., including 28-day compressive strength (full data model). Although the model is not perfect, we determine it is the best source of simulated data (see Note S2 for further detail). The alternative approaches aim to span competing techniques and varying numbers of hyperparameters. First, we evaluate Latin hypercube sampling (LHS), an approach that does not require a predictive model. Second, given their prevalence in the literature, we evaluate two standard GP models with two different kernel choices. The first uses a simple, standard approach where time and formulation are concatenated into a single input vector and used as input to a Matérn kernel. The resulting GP has three hyperparameters. The second uses a product kernel over time and formulation, resulting in five hyperparameters. Finally, we include our proposed aGP model without early stopping; this model has six hyperparameters. See Figure 4A for the summary of five approaches and the "comparison methodology" section for additional simulation detail.

Motivated by our result of 93% improvement in GWP within 28 days, we perform our comparisons by considering both the decrease in GWP given a 28-day budget as well as the amount of time required to achieve at least a 90% improvement in GWP. We stress that, despite only having four dimensions, our design space is rather large. If we were to consider only formulations that improve upon the optimal qualifying cement after initial data collection *and* restrict our search space to 95% RH through an exhaustive search, running four experiments at a time, the

Please cite this article in press as: Lin et al., Closed-loop optimization using machine learning for the accelerated design of sustainable cements incorporating algal biomatter, Matter (2025), https://doi.org/10.1016/j.matt.2025.102267

CellPress
OPEN ACCESS

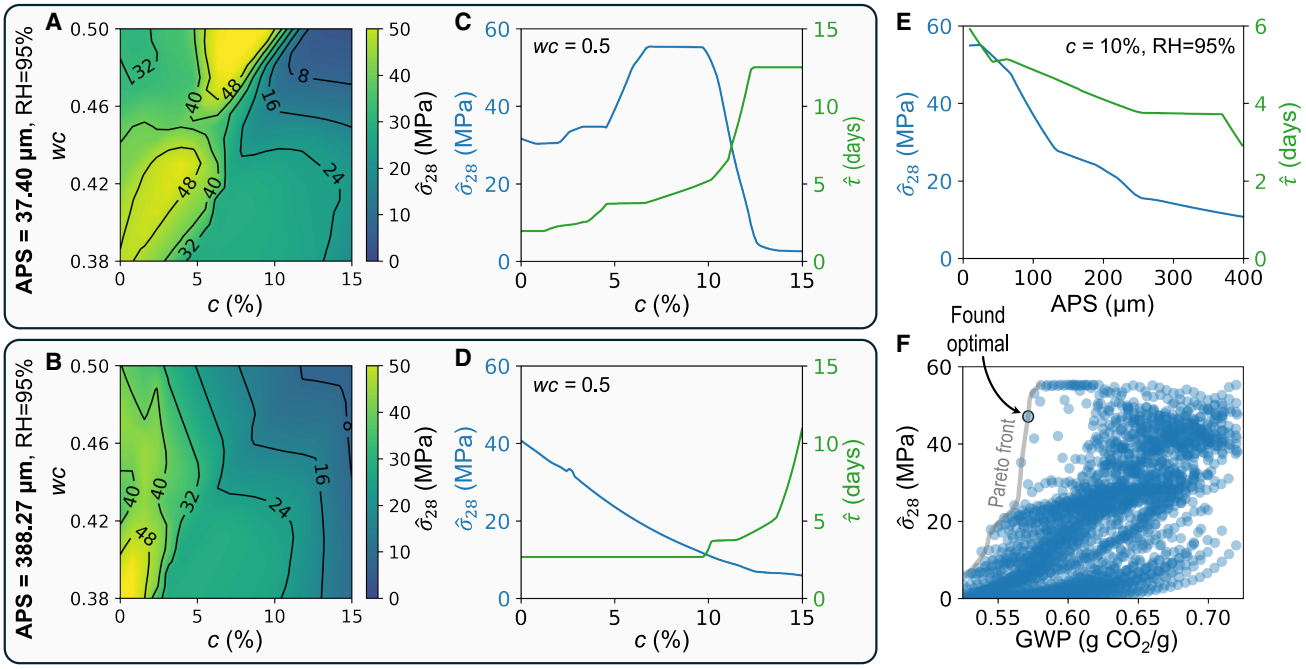

Figure 5. Data-informed knowledge from aGP model trained with the complete dataset

(A–D) At 95% RH, the predicted 28-day compressive strength of formulations at varying *Ulva* concentration *c* and water-cement ratio *wc* with (A) *APS* = 37.40 µm and (B) *APS* = 388.27 µm *Ulva* particles. Predicted 28-day strength $\widehat{\sigma_{28}}$ and characteristics time $\hat{\tau}$ at varying *Ulva* concentration at (C) *APS* = 37.40 µm and (D) *APS* = 388.27 µm.

(E) At *c* = 10% and *RH* = 95%, $\widehat{\sigma_{28}}$ and characteristics time $\hat{\tau}$ at varying *APS*.

(F) The trade-off relationship between predicted 28-day strength and GWP and the Pareto front.

complete data collection would take almost 11 years. Comparing the percentage of GWP improvement over time for different approaches as shown in Figure 4B, we see this time decrease to approximately 5 years by employing an LHS using the median of 1,000 repeated trials. LHS also results in 34% of the achievable improvement when restricted to a 28-day budget. Conversely, we observe 0% of the achievable improvement in 28 days when using standard GP approaches. However, these approaches do result in more rapid adaptation and achieve 100% of the GWP improvement in 196 and 168 days when using Matérn and product kernels, respectively. Finally, we note that, without early stopping, the aGP model achieves 45% of the GWP improvement in 28 days and 100% in 140 days. Although our closed-loop approach only achieved 93% of the GWP improvement, it was 5× faster than the next-best approach. Overall, we observe a clear advantage to both the use of the aGP model and the early-stopping criteria for accelerated design.

Data-informed bonding-structure-properties relationships

Given the success of the aGP model in closed-loop experimentation, we perform a *post hoc* analysis to better understand the relationships between the design space variables and compressive strength. For this analysis, we use the full data model, also used as the simulator, for our comparative analysis. This model is trained on all available data and is the highest-performing model (root-mean-square error (RMSE) = 5.02 MPa; see Figure S4A). Here, we vary elements of the design space and observe the predicted effect on compressive strength.

Focusing on the impact of *Ulva* concentration and *wc* on the 28-day strength (see Figures 5A and 5B), we observe a diagonal ridge of approximately constant strength along an increasing *Ulva* concentration and the *wc* line for smaller *APS* at the fixed humidity *RH* = 95%, indicating that higher *wc* is required at higher biomatter concentrations to achieve the same strength. Despite the presence of a valley between the ridges at approximately *c* = 5% and *wc* = 0.45 for *APS* = 2.86 µm (see Figure S4B) and 37.40 µm in Figure 5A, we hypothesize that the ridges of 48 MPa are continuous as we see the valley disappearing with increasing particle sizes (Figures 5B and S4C) and attribute the valley to the lack of data points at these specific conditions (around *c* = 5%, *wc* = 0.45). Because of the functional form of the mean function, $(\theta_l)_2$ can be interpreted as an approximation of the characteristic time τ. The characteristic time, reported in days, describes the required time for a formulation to reach 63% of the final strength.[18] We refer to the model's approximation as $\hat{\tau}$. As shown in Figures 5C and 5D at fixed *wc* = 0.5 and *RH* = 95%, for both *APS* values, $\hat{\tau}$ gradually increases with increasing *c* when $c \leq 10\%$ and then exponentially increases when $c > 10\%$. $\hat{\tau}$ of *Ulva* cements with *APS* = 388.27 µm is consistently lower than that with *APS* = 37.40 µm, suggesting a faster hydration rate with larger *Ulva* particles. Interestingly, the exponential increase in $\hat{\tau}$ at $c = 10 - 12.5\%$ for *APS* = 37.40 µm corresponds to the steep change in its

Please cite this article in press as: Lin et al., Closed-loop optimization using machine learning for the accelerated design of sustainable cements incorporating algal biomatter, Matter (2025), https://doi.org/10.1016/j.matt.2025.102267

28-day strength from 48 to 8 MPa (see Figure 5C), which indicates that exceeding that concentration threshold triggers a drastic change in hydration mechanisms. This rapid decrease in strength, seen in the small *Ulva* particles, is similar to the drastic strength reduction we previously reported for microalgae cements above 5 wt %.[18] This phenomenon may be related to our previously proposed hypothesis[18] for the retardation and long-term hindrance of hydration reaction attributed to the acidified carboxylic and hydroxyl groups of the algal carbohydrates with increasing biomatter concentrations.

Comparing the impact of *Ulva* concentration on strength at fixed $wc = 0.5$, green cements with $APS = 388.27$ μm particles present a monotonic decline in strength (Figure 5D), while those with $APS = 37.40$ μm show a strength peak above 30 MPa at $c = 5 - 10\%$ (Figure 5C). This peak of strength highlights the potential of optimizing low-carbon green cement with small *Ulva* particles but also implies a different hydration mechanism induced by varying particle sizes. Indeed, when investigating the effect of *Ulva* particle size on the strength and hydration speed at fixed $wc = 0.5$ and $c = 10\%$ in Figure 5E, $\hat{\tau}$ increases with decreasing particle size and therefore the hydration rate is slower with decreasing biomatter particle size and increasing surface area. Specifically, $\hat{\tau}$ of green cement with $APS = 37.40$ μm is around 2-fold greater than $APS = 388.27$ μm, indicating that the retardation effect of small *Ulva* particles on cement hydration is more pronounced than that of large particles. However, while the lower $\hat{\tau}$ derived from larger *Ulva* particles indicates the presence of more mature cement after the same curing period, their 28-day strength decreases with increasing particle size, which contradicts the conventional expectation of increased strength with a higher degree of hydration. This surprising trend suggests mechanisms other than the degree of hydration may govern the strength.

Interestingly, the effects of *Ulva* concentration and particle sizes on strength also have important impacts on the optimization of GWP. In Figure 5F, we display the predicted final strength and the respective GWP of all 2,520 formulations in the design space. We observe a relatively sparse distribution of data points in the region below GWP 0.62 g CO_2/g green cements and above 30.8 MPa of final strength, which corresponds to our target region for optimization. As the GWP is primarily determined by the concentration of *Ulva* (see Figure 1C), a higher *Ulva* concentration results in a lower GWP. However, at *Ulva* concentrations between 10% and 12.5%, the aGP model predicts the strength to be highly sensitive to the *Ulva* concentration; hence, few data points both meet the strength requirement and have a low GWP. This relationship manifests as a Pareto front, the boundary that delineates the highest possible strength for the lowest possible GWP, with a very high slope. Our closed-loop experimental design approach suggested the formulation of $(c = 10.5\%, wc = 0.5, APS = 37.40$ μm, $RH = 95\%)$ as the optimal. *Post hoc* analysis indicates that this point is sub-optimal but is indeed on the Pareto front. Interestingly, $c = 11\%, wc = 0.5, APS = 2.86$ μm, $RH = 95\%$ is also a qualifying formulation but not on the Pareto front due to the impact of milling energy demonstrating the important role of particle size in calculating GWP (see Figure S5).

To provide a physical understanding of the predicted particle size effects of *Ulva* on cement's hydration reactions, we conducted thermogravimetric analysis (TGA) on composites with $c = 10\%$ and $wc = 0.5$ and particle sizes $APS = 388.27$ and 37.40 μm. This method enables the characterization of the hydration product, calcium hydroxide ($Ca(OH)_2$) which degrades between 380°C and 520°C, and calcium carbonate ($CaCO_3$) degrading between 600°C and 780°C.[38] As shown in Figures 6A and 6B, the $Ca(OH)_2$ content of the *Ulva* cements is identical between different particle sizes in the early age at around 3 wt %, yet the decomposition temperature of $Ca(OH)_2$ of *Ulva* cements with $APS = 37.40$ μm is slightly lower than with $APS = 388.27$ μm by 10°C, implying a smaller crystal size of $Ca(OH)_2$. As confirmed by the X-ray diffraction (XRD) patterns in Figure 6C and peak analysis in Table S2, on day 7 the portlandite ($Ca(OH)_2$) peaks at 18.1°, 34.1°, and 47.1° have a 37.8% lower intensity and 14.7% larger full width at half maximum (FWHM) for *Ulva* cements with $APS = 37.40$ μm compared to $APS = 388.27$ μm, confirming the smaller crystal size induced by smaller *Ulva* particles. Meanwhile, on day 7, the $APS = 37.40$ μm *Ulva* results in 2 wt % higher content of $CaCO_3$, as quantified from TGA, and 11.8% higher peak intensity and 50% larger calcite ($CaCO_3$) crystal size, as quantified by the XRD peak at 23.1°, compared to $APS = 388.27$ μm, suggesting that calcium-based hydration products are more accessible for carbonation in the microstructure of composites with smaller particles.

Indeed, scanning electron microscopy (SEM) images (Figures 6D–6G) confirm the distinct microstructures of *Ulva* cements with varying particle sizes. Large voids in the range of hundreds of μm are present in $APS = 388.27$ μm samples (Figure 6D), in contrast to the smaller voids of tens of μm in $APS = 37.40$ μm samples (Figure 6F). These apparent interfacial gaps between the cement matrix and the large *Ulva* particles may be caused by the volume change of biomatter. We hypothesize that the cells take up and release some of the water in the adjacent cementitious matrix for continuous hydration, while the rest of the water taken up slowly evaporates after the cement is hardened, leading to the biomatter shrinkage. In contrast, the small *Ulva* particles are better incorporated in the cement matrix with clear *Ulva* cell and tissue imprints in the cement matrix (see Figures 6F and 6G). The presence of fibrous crystals distributed across the biomatter and cement matrix results in a relatively loose network of hydration products with smaller interfacial gaps, as shown in Figure 6G. This micromorphological difference may explain the higher $CaCO_3$ content in the *Ulva* cements with small biomatter particles, as the cement hydration products are more accessible to air compared to the dense hydrated cement matrix with the additions of large *Ulva* particles. However, since the $CaCO_3$ particles function as inert fillers and the thermal degradation profiles of *Ulva* cements with different biomatter particle sizes are identical at day 28, we hypothesize that the strength differences are due to variations in fracture behavior induced by the micromorphological differences. As shown in Figure S6, the $APS = 37.40$ μm samples experience a classic semi-brittle failure and have a three times higher compressive strength than the $APS = 388.27$ μm samples. This suggests the large interfacial gaps present in the *Ulva* cements with large *Ulva* particles act as stress concentrators and fracture initiation points, triggering crack development and crumbling at lower stress. In contrast, the interconnected hydration products

Please cite this article in press as: Lin et al., Closed-loop optimization using machine learning for the accelerated design of sustainable cements incorporating algal biomatter, Matter (2025), https://doi.org/10.1016/j.matt.2025.102267

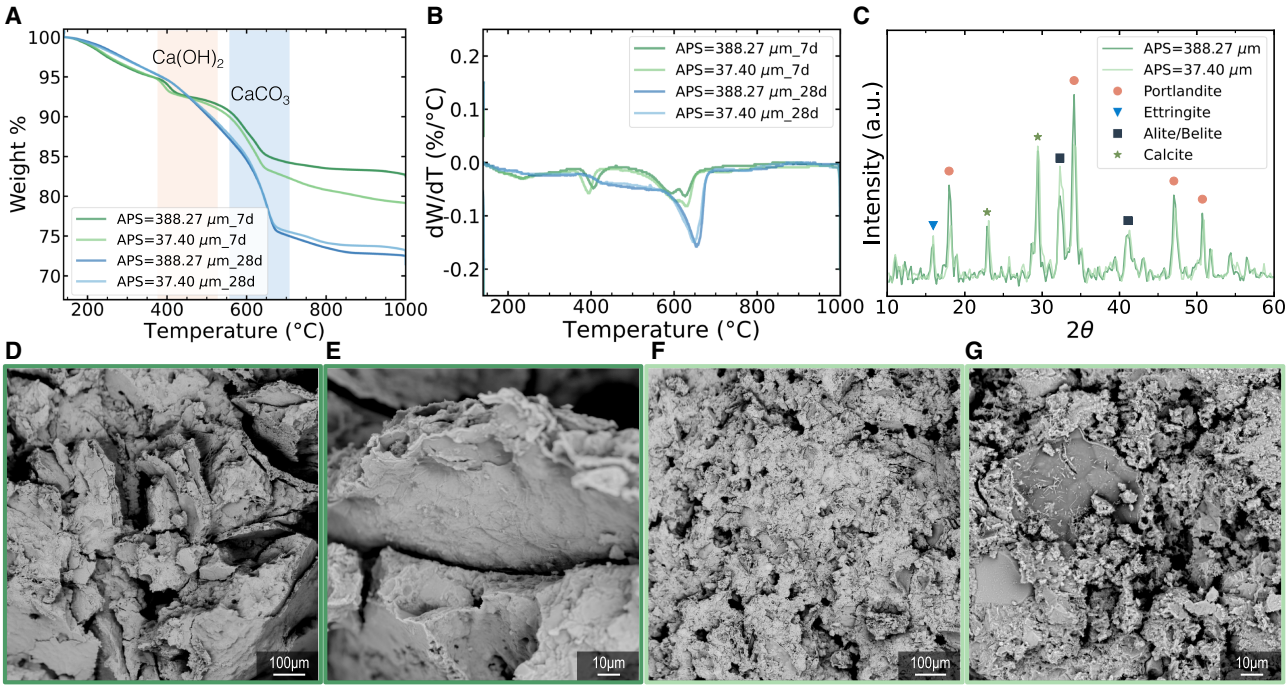

Figure 6. Particle size effects on the hydration and microstructure of *Ulva* cements

(A and B) (A) The mass loss profiles through TGA and (B) derivative thermogravimetry (DTG) curves of *Ulva* cements at c = 10%, wc = 0.5, RH = 95%, and APS, respectively, of 388.27 and 37.40 μm on day 7 and 28.

(C) The XRD patterns of *Ulva* cements with the same formulations on day 7.

(D–G) The SEM images of *Ulva* cements at c = 10%, wc = 0.5, RH = 95%, and APS = 388.27 μm (D and E) and APS = 37.40 μm (F and G).

and smaller voids in the small particle-sized *Ulva* cements lead to higher strength.

Based on these characterized material properties, we have shown that the aGP model is capable of capturing the impact of specific variables that are otherwise difficult to characterize without extensive studies. For example, the smaller size of portlandite caused by the small *Ulva* particles at an early age substantiates the longer characteristic time ($\hat{\tau}$) required for green cements with small biomatter particle size, as suggested by the aGP model. This perspective on hydration rate and strength evolution highlights the unique insights discoverable via the use of a domain-informed mean function with an aGP. Moreover, these impacts of biomatter particle sizes on the hydration mechanism and strength further enable us to depict the trade-off between increased GWP from milling and increasing strength over time, as well as decreasing GWP with biomatter concentration and sacrificing strength. The above demonstration of ML-informed discovery reveals the potential not only for expanding the fundamental understanding of advanced green cements during material optimization but also for modulating the material's performance and environmental impact simultaneously.

DISCUSSION

Our analysis demonstrates the value of closed-loop experimental design for green cements. In 28 days, our approach discovered a green-cement formulation achieving 93% of the potential reduction in GWP, a 21% decrease compared to standard OPC, representing an estimated 5× speed-up over the next best approach and saving 112 days of experiment time. This success highlights the active-learning capabilities of our ML model, allowing us to make real-time experimental selections without access to 28-day strength measurements and by relying on a limited training dataset, thus providing true validation of our methodology. Although previous studies have aimed to discover low-carbon cements,[25,26,33,39] ours is the first to focus on biomatter substitution, rather than SCM. While existing empirical[40] and some ML-based methods[25,26] can estimate later-age strength using early-age measurements, these approaches are tailored to well-established cementitious materials incorporating SCM. Building on this foundation, we develop a more generalizable predictive model via aGP, which is better suited to capture not-yet-characterized non-linear relationships presenting in novel material systems. Our methodology tackles the challenges posed by the complex interactions between biomatter components and the cementitious matrix, such as concurrent effects from particle size, poor interfacial adhesion, new reaction products, and modified carbonation kinetics, all influencing the strength development in this class of green cements. Moreover, our design framework is not specific to green cements, and can be used to optimize formulations leveraging other sustainable materials as well.

Many experimental and computational design choices were made during our study. In this section, we interrogate some of

these choices. We selected a fixed, discrete design space. During the closed-loop optimization, we notice that the selected experiments rapidly focus on *wc* = 0.5, which is the boundary of the *wc* design space. This high *wc* demand for green cement points to the known high water uptake capacity of *Ulva*, stemming from its native component hydrophilicity, abundant hydrogen bonding sites, and tissue structure that allows for swelling. Expanding the *wc* bound might enable the discovery of a green cement with even lower GWP. However, it is not clear if this would indeed be beneficial, as a higher *wc* could also lead to a more porous structure and consequently lower strength. While we chose a constant design space in this study, in real-world applications, the design space could be expanded during testing. Similarly, we note that *RH* also had fast convergence to a boundary condition of 95%, although *RH* is a truly bound variable. Even though *RH* has relatively minimal impacts on GWP, we do report large effects on strength. This observation points to the need for careful consideration when selecting the design space, particularly not only considering GWP but all optimization variables. We note that the inclusion of *RH* introduced an experimental constraint, as, in our current lab setup, experiments in each round were required to be performed at the same *RH* if they were to be performed in parallel.

There are alternative approaches for defining the acquisition function, which is used to select which formulations in the design space are tested. Instead of explicitly considering GWP, we could have focused exclusively on determining which formulations were qualifying (i.e., meet the strength criterion) and then selected the cement with the lowest GWP from this set. This choice is also reasonable because there is no uncertainty in the estimation of GWP. However, we did not pursue this approach as our assumption was that this formulation of the problem does not take advantage of addressing the strength and GWP aims simultaneously, resulting in a larger set of formulations of interest at each round and likely a more challenging optimization.

Based on both predictive performance and closed-loop testing, the aGP model class is well suited to the problem we are tackling. One of the key advantages of the aGP approach is its mean function, which enables a valid parameterization of the compressive-strength evolution and provides a useful constraint to better learn from small datasets. This parameterization also enables *post hoc* analysis, which allows us to draw connections between the learned hyperparameters and the underlying physical phenomenon. In contrast, alternative models often overfit to small sample size and lack intuitive interpretability. However, the aGP does come with the risk that the mean function does not well approximate true trajectories. This could become a more major issue in the case where model errors are not independent and identically distributed but are a function of time. A failure mode would be the case where early time points are well modeled and late time points are not, leading to the introduction of bias via the early-stopping criteria. In practice, it is critical to evaluate model performance both overall and as a function of time to avoid these issues and inform an appropriate choice of early-stopping criteria. Another significant advantage is the aGP model's ability to capture the highly non-linear response of compressive strength to the design space. For example, there is a sharp decline in compressive strength from 10% to 12% *Ulva* concentration. Standard GP models rely on smoothness assumptions, which retrospectively appear ill-suited to green cements. Instead, the aGP model captures these relationships through a multi-layer perceptron (MLP) model, allowing for non-linearities. As the MLP's depth and width, which in turn are related to the model's ability to model non-linear functions, are learned using the initial data collection, we expect this class of model is well-posed to capture a flexible class of relationships.

In this study, we applied a point-based strength criterion and determined if a formulation met the criterion based on the mean of the measured data. In practice, ASTM C94[41] and ACI 214R[42] suggest deciding the required average compressive strength after considering the variation of data and specified strength. Our framework could be adapted to consider probabilistic criteria for strength, which would more naturally account for this variation; however, we leave this to future work. In addition, we used a simplified deterministic function for the GWP characterization in this study, which may not be generalized in applications requiring quantified emissions in the life-cycle inventory. In practice, LCA studies often adopt various data sources and face challenges related to non-standardized analysis procedures and inconsistent scopes, leading to data discrepancies.[43] The aGP model class offers opportunities to incorporate the variations found in LCA analyses, providing a distribution in the environmental impact dimension and enabling a more comprehensive exploration of sustainable materials. These alternative approaches to our experimental and computational choices could be interesting to investigate further in future work.

In conclusion, our study, motivated by mitigating GHG emissions of conventional cement, has demonstrated that a closed-loop design framework assisted by the aGP model and early stopping can speed up the discovery of novel green cements utilizing carbon-negative biomatter. The model's ability to integrate domain knowledge and predict time-trajectory properties shows potential to extrapolate to other cementitious materials. We expect this design framework to further support the accelerated design for advanced sustainable materials.

METHODS

Materials

Commercially available Type I/II Portland cement (SAKRETE, Charlotte, NC, USA) abiding by ASTM C150[34] was used as the cement matrix and incumbent material. The chemical composition of the Portland cement determined by X-ray fluorescence and TGA is shown in Table 2. *Ulva expansa* was provided by the Marine and Coastal Research Laboratory of the Pacific Northwest National Laboratory - Sequim (Seattle, WA, USA), where *Ulva* was cultivated in natural seawater in indoor ponds.

Design space and initial data collection

The design space explored to optimize green cements includes water content (characterized water to cement mass ratio, [*wc*], *Ulva* concentration [*c*], average particle size [*APS*], and the humidity of the curing chamber [(*RH*]). Ranges of 0.38–0.5 with a step size of 0.02 and 0.5 to 15 with a step size 0.5 are investigated for water-cement ratio and *Ulva* concentration, respectively.

Table 2. Oxide content and loss on ignition (wt %) of type I/II Portland cement used in this paper

CaO	SiO_2	SO_3	Al_2O_3	MgO	Fe_2O_3	K_2O	Na_2O	LOI
67.14	14.00	9.68	3.51	1.70	2.81	0.89	0.28	2.63

Particle size distributions of 1–30 (*APS* = 2.86, *P*80 = 8.5 μm), 10–150 (*APS* = 37.4, *P*80 = 98.7 μm), 70–400 (*APS* = 138.49, *P*80 = 357.0 μm), and 200–1,000 μm (*APS* = 388.27, *P*80 = 849.6 μm) and humidity values of *RH* = 10%, 50%, and 95% were also explored. The initial samples were selected based on a Latin hypercube experimental design strategy considering only a subset of *Ulva* content values, specifically 0.5%, 1%, 5%, and 15%. A total of 24 experiments were selected and five replicates were tested per time point to train the initial model (see Table S4 for selected experiments; see the "prediction of compressive strength" section for modeling details).

Preparation of the green cement samples

Ulva was collected from the cultivating pool, washed with salt water at room temperature, and then dehydrated. The dry *Ulva* tissue was first ground by a coffee grinder (Hamilton Beach Fresh Grind, Southern Pines, NC, USA) for 20 s per 6 g. Sieve no. 35 (500 μm), no. 50 (297 μm), and no.100 (149 μm) were then used to filter two particle sizes of 388.27 ± 208.97 μm and 138.49 ± 73.59 μm. Next, the *Ulva* particles passing through sieve no.100 were ground by a vertical high-energy planetary ball mill (MSE PRO 1L MA0103, MSE Supplies, Tucson, AZ, USA) for 30 min at 400 rpm for particle size of 37.40 ± 20.71 μm and at 500 rpm for that of 2.86 ± 1.87 μm. The *Ulva* of the targeted particle size was premixed with cement powder at the selected concentrations between 0.5 and 15 wt % by weight of the total dry mass, using a planetary mixer (SpeedMixer DAC 330-100 PRO, FlackTek, Landrum, SC, USA) to mix for 30 s at 1,500 rpm. Next, deionized water was added to the mixture to achieve the desired *wc*, and the mixture was further homogenized by the same speed mixer for 3 min at 1,500 rpm. Then, the mixed paste was cast into rubber molds to produce samples in the dimensions of $10 \times 10 \times 10\ mm^3$ for compression tests. A vibration table (no. 1A vibrator, Buffalo Dental Manufacturing, Syosset, NY, USA) was used when casting the samples to remove macroscopic air bubbles. Right after casting, the samples were covered with plastic films and placed in a moisture-controlled chamber to cure at the desired humidity (10%, 50%, or 95% RH) for 7 days and then stored in the ambient environment from day 7–28.

Compressive-strength measurement

Compression tests were conducted on five samples for each mixture on the designated testing date using a universal test frame (Autograph AGS-X 10 kN, Shimadzu Scientific Instruments, Columbia, MD, USA) with a 5 kN load cell. The samples were compressed at a constant stress rate that complies with ASTM C109/C109 M.[44] The maximum compressive stress value in the stress-strain curve is noted as the ultimate compressive strength. A complete set of time points for a sample is days 2, 4, 7, and 28. All initial dataset collection measured all time points. During closed-loop optimization, days 2 and 28 were always measured and days 4 and 7 were measured only when early termination was not recommended (see the "accelerated optimization algorithm" section).

Attributional LCA: Deterministic model for specific CO_2 emissions

In this section, we describe and attribute relevant values to each term of the *GWP* assessment provided in Equation 1. It should be emphasized that the values of CO_2 emissions can vary widely depending on location and the type of available energy sources. Specific emissions chosen in this study might not accurately represent any green-cement fabrication method.

CO_2 emissions of anhydrated OPC

The emission of anhydrated OPC powder was taken as a typical value reported in literature of $\mu_{OPC} = 1$ g CO_2/g OPC.[45]

CO_2 emissions of water

Water-related CO_2 emissions vary significantly depending on local water availability, but reported values are always significantly smaller than OPC CO_2 emissions. In our model, we took a reasonable average value of $\mu_{water} = 0.0004$ g CO_2/g water (https://www.brightest.io/calculate-carbon-footprint-water-emissions). Since water emissions are small, we neglect the possibility of water evaporation during cement hydration (i.e., we assume that the final mass of the hydrated green cement is equal to the sum of the masses of each component used to fabricate the cement). Note that, since water has a much lower carbon footprint than OPC, the GWP of hydrated cements will depend on the water-cement ratio. Indeed, increasing the amount of water will increase the final mass of the hydrated cement, without significantly increasing its GWP, thereby globally reducing specific GWP (in g CO_2/g hydrated green cement). This decreasing behavior is observed in the top left plot of Figure 1C.

CO_2 emissions of Ulva powder

The specific CO_2 emissions associated with the *Ulva* content of the green cements can be separated into two terms such that

$$\mu_{Ulva} = \mu_{raw.Ulva} + \mu_{mill}(P80), \qquad \text{(Equation 3)}$$

where $\mu_{raw.Ulva}$ corresponds to the upstream emissions attributed to the dry *Ulva* flakes received and used as raw material, and $\mu_{mill}(P80)$ to the emissions associated with energy consumption necessary to grind the raw *Ulva* down to a smaller particle size (characterized by the 80% undersize by weight fraction, *P*80).

Negative CO_2 emissions of raw Ulva. Upon growth, *Ulva* takes up CO_2 from the atmosphere through photosynthesis. The specific carbon content contained in seaweed depends on species and cultivation conditions. In this study, we make the reasonable assumption that each gram of dry *Ulva* contains 30 wt % of carbon (C) based on other typical carbon content in algae in literature,[46,47] corresponding to an uptake of 1.1 grams of CO_2 per gram of dry *Ulva*. This attractive CO_2 uptake is mitigated by the subsequent steps necessary to make *Ulva* useful to fabricate green cements, such as drying down the harvested (wet)

seaweed. In an ideal (yet realizable) scenario, Koesling et al.[48] provide an estimate of the carbon impact attributed to seeding, deployment, harvesting, transport, and drying of the seaweed, resulting in total CO_2 emissions of 0.41 g CO_2/g dry seaweed. Accounting for the intrinsic negative emission of −1.1 g CO_2/g dry *Ulva* and the positive processing emissions of 0.41 g CO_2/g dry seaweed, the resulting CO_2 emission attributed to the raw dry *Ulva* used in this study is finally $\mu_{raw.Ulva} = -0.69$ g CO_2/g dry raw *Ulva*. Note that a negative specific emission value corresponds to beneficial carbon sequestration.

CO_2 emissions of milling. The raw *Ulva* used in this project was received in the form of dried flakes of millimetric size. The mechanical energy required to grind down the particles to a smaller *APS* is responsible for additional positive CO_2 emissions. A common approach to predict the milling energy of particles is to use the Bond work index, W_i[37]. This work index, expressed in kJ/kg, corresponds to the energy required to mill particles from theoretical infinite size down to a passing size of 100 μm. More generally, this approach enables the prediction of the energy necessary, E_{mill} (in kJ/g of powder), to mill down a powder feed of given 80% passing size ($F80$, in μm) down to a target 80% passing size ($P80$, in μm) using the following equation:

$$E_{\text{mill}} = 10W_i \cdot \left(\frac{1}{P80} - \frac{1}{F80}\right). \quad \text{(Equation 4)}$$

The precise determination of W_i of our *Ulva* goes beyond the scope of this paper, as this parameter is only meaningful when measured at an industrially relevant scale. We, therefore, approximate our W_i as a value reported in the context of rice milling by Ngamnikom and Songsermpong,[49] where the authors measured a specific energy of 0.42 kJ/g to bring rice particles down to an average size of 95 μm through dry grinding with a hammer mill. In our calculations, we used a feed 80% passing size of $F80 = 1,000$ μm. Finally, we convert this specific energy to specific CO_2 emissions assuming that electric energy is produced from natural gas, yielding emissions of 0.12 g CO_2/kJ based on US electricity net generation and resulting CO_2 emissions using natural gas in 2022 (https://www.eia.gov/tools/faqs/faq.php?id=74&t=11).

CO_2 emissions associated with curing in a humidity-controlled environment

For completeness, the CO_2 associated with the environmental relative humidity during curing of the green cements was also included in the model. However, given the vast variety of approaches to ensure humid, or dry, environments, we opted for a simple model describing μ_{RH}. We assumed that no intervention is needed to cure the cements at $RH = 50\%$, meaning that no additional CO_2 emissions are included at this relative humidity. On the other hand, water input is necessary to achieve relative humidities larger than 50%. Specifically, we assume that, for each gram of hydrated green cement, a gram of water would be necessary to achieve $RH = 100\%$. The CO_2 emissions associated with a humid environment are therefore proportional to μ_{water}. Conversely, we make the assumption that symmetric CO_2 emissions are associated with drying the environment (i.e., that emissions at 0% are equal to emissions at 100%). Finally, the term μ_{RH} reads

$$\mu_{RH}(RH) = 2\,\mu_{\text{water}}|RH/100 - 0.5|. \quad \text{(Equation 5)}$$

The influence of *RH* is represented in the bottom right plot of Figure 1C. We observe that the GWP of green cements is almost unaffected by the relative humidity. The magnification along the GWP axis presented in the inset shows that, in this case ($wc = 0.45$, $c = 5\%$, $P80 = 37.4$), the influence of *RH* is below 0.005 g CO_2/g hydrated green cement between 50% and 100%.

SEM

Samples were coated with 4 nm of gold in a sputter coater (108 Manual, Ted Pella, Redding, CA) prior to imaging in the SEM (Phenom ProX Desktop SEM, Thermo Fisher Scientific, Waltham, MA, USA) at an accelerating voltage of 10 kV. To conduct the particle size analysis, ImageJ was used for post-processing on the acquired images.[50]

TGA

Samples (6–10 mg) were heated in platinum crucibles from ambient temperature to 1,000°C using a TGA instrument (D550, TA Instruments, New Castle, DE, USA) under a 25-mL/min flow of nitrogen gas. The temperature was first increased to 140°C at a rate of 10°C/min and was kept isothermal for 30 min to evaporate the absorbed water in samples, and was then further increased to 1,000°C at a rate of 10°C/min.

XRD

The X-ray diffraction measurement was conducted using a D8 Advance XRD, Bruker, Billerica, MA, USA with Cu Kα X-ray radiation (wavelength 1.5406 Å). The diffraction patterns were collected from 5° to 70° 2θ with a step increment of 0.02° and a collection of 0.07 s/step. The XRD analysis was done based on the MDI-500 library (JADE 8.3, Materials Data, Livermore, CA).

Prediction of compressive strength

We selected a class of GP models to predict the compressive strength of green cements as a function of time, composition, and curing conditions. A GP describes a distribution over functions of the form $f : \mathcal{X} \to \mathbb{R}$, any finite set of which follow a Gaussian distribution with mean $[\mu]_i = m(x_i)$ and covariance $[\Sigma]_{ij} = k(x_i, x_j)$, where x_i and x_j are two elements of input x. For a more complete introduction to GP models, we refer to Williams and Rasmussen.[51]

For our application, we specifically leverage amortized GPs. We assume that the compressive strength of each cement is modeled as a noisy output of a GP evolving in time

$$\widehat{\boldsymbol{\sigma}}_i = f_i(\mathbf{t}_i) + \varepsilon_i(\mathbf{t}_i), \quad \text{(Equation 6)}$$

where i denotes a particular sample, and $\mathbf{t}_i, \widehat{\boldsymbol{\sigma}}_i \in \mathbb{R}^{J_i}$ are the time points and compressive strengths, respectively. Note that we use $\widehat{\sigma}$ to differentiate the model predictions from measurements throughout the manuscript. The GP f is then specified,

$$f_i \sim \mathcal{GP}\left(m(\mathbf{t}_i;\theta_i), k\left(\mathbf{t}_i, \mathbf{t}_i';\theta_i\right)\right), \quad \text{(Equation 7)}$$

Please cite this article in press as: Lin et al., Closed-loop optimization using machine learning for the accelerated design of sustainable cements incorporating algal biomatter, Matter (2025), https://doi.org/10.1016/j.matt.2025.102267

$$m(\mathbf{t}_i;\theta_i) = (\theta_i)_1\left(1 - \exp\left(-\frac{\mathbf{t}_i}{(\theta_i)_2}\right)\right), \quad \text{(Equation 8)}$$

$$k(\mathbf{t}_i,\mathbf{t}_i';\theta_i) = (\theta_i)_3 \exp\left(-\frac{|\mathbf{t}_i - \mathbf{t}_i'|}{(\theta_i)_4}\right), \quad \text{(Equation 9)}$$

$$\theta_i(\mathbf{z}_i) = h_\phi(\mathbf{z}_i), \quad \text{(Equation 10)}$$

where θ_i are the hyperparameters of the GP, $\mathbf{z}_i \in \mathbb{R}^d$ describes the composition and curing conditions of sample i, and h_ϕ is a function that predicts the GP hyperparameters, called the hyperparameter network. This approach differs from classic GP models where hyperparameters would be learned for each individual formulation and instead learns h_ϕ, which maps the formulation and curing conditions to hyperparameters. This model formulation allows for informative priors for unseen formulations while also enabling a time-based parameterization of the mean function. The particular choices for the mean and kernel functions are motivated by domain knowledge. Specifically, the parameterization of the mean function, $m(\mathbf{t}_i;\theta_i)$ (see Equation 8), is motivated by empirical evidence of the trajectory of algae-based cements. This time evolution corresponds to an initial linear increase, followed by a plateauing strength behavior at longer times as proposed by Lin et al.[18] The parameterization of the kernel function, $k(\mathbf{t}_i,\mathbf{t}_i';\theta_i)$ (see Equation 9), is motivated by the observation of sharp transitions in the compressive-strength trajectory. The observation noise model $\varepsilon_i(\mathbf{t}_i)$ is also informed by domain knowledge

$$\varepsilon_i(\mathbf{t}_i) \sim \mathcal{N}(0, v_{it}), \quad \text{(Equation 11)}$$

$$v_{it} = (\theta_i)_5\left(1 - \exp\left(-\frac{\mathbf{t}_i}{(\theta_i)_6}\right)\right), \quad \text{(Equation 12)}$$

where θ_i are also the output of the hyperparameter network. The parameters of the hyperparameter network h_ϕ are learned by maximization of the log marginal likelihood of the training data

$$\mathcal{L}(\phi) = \sum_{i=1}^{N} \log p(\widehat{\boldsymbol{\sigma}}_i|\mathbf{t}_i,\mathbf{z}_i,\phi). \quad \text{(Equation 13)}$$

The initial model is fitted using the round 0 dataset, as described in the "design space and initial data collection" section. Four experiments are held out as a test set and a parameter sweep over the number of the layers and the latent dimension of the MLP is performed with 10 random restarts for each setting. Specifically, numbers of layers in $\{2,4,8,16,32\}$ and latent dimensions in $\{10,20,40\}$ are tested. Results are stored for 50, 100, 150, 200, and 250 optimization steps. The final model was selected based on test data likelihood and has 16 layers with a hidden dimensionality of 10.

Accelerated optimization algorithm

Our experimental design objective is to find the green cement with the lowest GWP while still meeting the 28-day strength constraint of 30.8 MPa within a 28-day experimentation budget. Although a classic design of experiments such as Latin hypercube or factorial design would provide optimal coverage of the design space, we use a closed-loop experimental design that follows a Bayesian optimization approach[52] with additional consideration for early termination of experiments to exploit our knowledge about the relationship between formulation and compressive strength. As outlined in Figure 1, our proposed optimization procedure consists of two iterative loops: one to select formulations to test (outer loop) and one to determine the duration of the experiment (inner loop). To select experiments, we jointly consider which formulations are likely to meet the strength criterion and which formulations improve upon the GWP. Constraint-weighted acquisition functions[53] and constrained predictive entropy search[54] were both plausible approaches, but we selected the former based on straightforward integration with early stopping as described below.

Experiments are selected based on a constraint-weighted acquisition function[53] that considers the improvement in GWP, subject to meeting the strength criterion ($\sigma_{28} \geq 30.8$ MPa). The predicted strength is estimated using the amortized GP model (see the "prediction of compressive strength" section). We note that we need not consider the *expected* improvement in GWP, as GWP is assumed to be a deterministic function of cement formulation. The mathematical expression for the acquisition function is therefore

$$A(z_i) = p(\widehat{\sigma}_i|t = 28, z_i, \phi)(GWP(z^*) - GWP(z_i)), \quad \text{(Equation 14)}$$

where z^* is the cement formulation with the current best (lowest) GWP and all other terms are as defined above. This choice of acquisition function balances the potential improvement, as captured in the second term, with the likelihood of meeting the strength constraint, as captured in the first term. This implies that highly uncertain formulations (those with low probability of meeting the constraint) will be selected when they provide a sufficiently large potential payoff (i.e., a very large decrease in GWP). Because of the high correlation between GWP and strength, in practice, we first test whether any of the mean predictions meet the strength criterion, and, if so, select four experiments only from this subset using the acquisition function.

To accelerate the optimization process, we employ an early-stopping approach that enables the early termination of mechanical testing of cement samples under specific conditions, bypassing the full 28-day waiting period before the next optimization iteration. The early-termination criteria depends on whether the proposed cement is or is not a *qualifying* formulation (i.e., whether it is predicted to meet the strength criterion or not). For qualifying cements, when the first compressive strength measurements are recorded at 2 days, a posterior probability of 28-day strength surpassing the criterion is calculated. The RMSE of the prior prediction, before observation, as compared to the observed data, is also calculated. If the RMSE is less than 6 MPa and the posterior probability of qualifying is at least 60%, the experiment is terminated and *accepted*, recorded as a qualifying formulation. Otherwise, the experiment continues and this procedure is repeated at 4 and 7 days. The maximum

duration for an experiment is 7 days. For proposed cements that are not qualifying, if the RMSE is less than 6 MPa and the posterior probability of qualifying is less than 20%, the experiment is terminated and *rejected*, recorded as a non-qualifying formulation. Furthermore, if the RMSE is greater than 6 MPa but the posterior prediction of 28-day strength is less than the initial prediction, the experiment is recorded as a non-qualifying formulation and terminated. The RMSE threshold (of 6 MPa) was determined based on the standard deviation of compressive-strength measurements for qualifying cements in the initial round of experimentation. Both the posterior probability and RMSE thresholds were selected to be conservative as compared to the true criterion of 50%. By using both, we incorporate both a retrospective consideration of our selection (via RMSE) and a future-looking consideration of the likelihood of qualifying (via the posterior probability). Experimental time and resources prevented us from exploring more settings.

Comparison methodology

To demonstrate the value of our proposed approach, we compare it to other experimental design methods. We consider four alternative settings: LHS, standard GP, GPs with domain-inspired kernels, and amortized GPs without early stopping. In all cases, we consider both how much of the realizable improvement in GWP can be achieved in the alternative setting with the same time budget of 28-day as well as what time budget would have been required to match the improvement in GWP of our analysis. To simulate the results of experiments that were not performed, we use an amortized GP model trained on all collected data, 44 samples in total, which we refer to as the full data model (see Tables S1–S4 for full data description). It should be noted that other predictive models were considered, yet the aGP model consistently outperformed other approaches and was therefore selected as the best possible source of ground truth (see Note S2). In the following paragraphs, we describe each of the alternative methods.

To compare with LHS, we selected the subset of experiments that were a possible improvement in GWP after round 0 and only experiments with 95% humidity. The humidity condition was added to simplify selection as only one humidity can be tested at a time; the impact of this restriction should only be favorable to the LHS approach. In the fixed-time budget setting, we perform 1,000 trials of selecting four experiments and record whether the formulation meets the strength criterion and, if so, the corresponding GWP. In the fixed-improvement setting, we consider doubling the number of experiments until we reach a median improvement in GWP that is at least as good as our proposed method.

To compare to a standard GP model, we concatenate each formulation with its corresponding time point and fit the model using a Matérn kernel, zero-mean function, and Gaussian independent and identically distributed (i.i.d.) noise. Predictions are made using the posterior, and the acquisition function remains the same (see Equation 14). New data are simulated from the aGP model and added to the GP after each round, updating the posterior. A GP model with a product kernel over formulation, modeled with a radial basis function kernel, and time, modeled with Matérn kernel, is also considered as a more domain-inspired approach.

RESOURCE AVAILABILITY

Lead contact

Please contact Dr. Eleftheria Roumeli (eroumeli@uw.edu) with all questions and requests.

Materials availability

All materials generated in this study are available from the lead contact upon reasonable request.

Data and code availability

- All relevant data supporting the findings of this work are available in this article and supplemental information.
- The source code supporting the findings of this study is openly available at GitHub at: https://github.com/roumelilab/ML-Optimization-Algal-Cements.

ACKNOWLEDGMENTS

The authors thank Scott Edmundson from Pacific Northwest National Laboratory, WA, USA for providing *Ulva* materials and Esther Nicolaou for assisting in the mechanical testing. Part of the characterizations were performed at the Washington Clean Energy Testbeds, a facility operated by the University of Washington Clean Energy Institute. This material is based in part upon work supported by the state of Washington through the University of Washington Clean Energy Institute. M.-Y.L., P.G., and E.R. acknowledge financial support in the form of gift funds from Microsoft Research.

AUTHOR CONTRIBUTIONS

M.-Y.L., K.S., and P.G. designed the study, including defining the design space, specifying the ML model, and determining the experimental flow. M.-Y.L. prepared samples and collected experimental data. P.G. designed the model to evaluate GWP. K.S. developed the training code, operated and trained the model, and exported predictions. M.-Y.L., K.S., and P.G., analyzed the results, wrote the manuscript, and prepared it for submission. E.R. contributed project supervision, funding acquisition, review of results, edits, and writing–review & editing of the manuscript.

DECLARATION OF INTERESTS

The authors declare no competing interests.

SUPPLEMENTAL INFORMATION

Supplemental information can be found online at https://doi.org/10.1016/j.matt.2025.102267.

Received: September 23, 2024
Revised: February 28, 2025
Accepted: June 10, 2025

REFERENCES

1. Intergovernmental Panel on Climate Change (IPCC) (2023). Climate Change 2022 - Mitigation of Climate Change: Working Group III Contribution to the Sixth Assessment Report of the Intergovernmental Panel on Climate Change (Cambridge University Press).
2. Adams, M., Burrows, V., Richardson, S., Drinkwater, J., Gamboa, C., Collin, C., Den, X., Riemann, L., Porteron, S., and Secher, A. Bringing embodied carbon upfront: Coordinated action for the building and construction sector to tackle embodied carbon. Tech. Rep. World Green Building Council (2019).
3. Andrew, R.M. (2019). Global CO_2 emissions from cement production, 1928–2018. Earth Syst. Sci. Data *11*, 1675–1710. https://doi.org/10.5194/essd-11-1675-2019.

4. Miller, S.A., Horvath, A., and Monteiro, P.J.M. (2016). Readily implementable techniques can cut annual CO_2 emissions from the production of concrete by over 20%. Environ. Res. Lett. *11*, 074029. https://doi.org/10.1088/1748-9326/11/7/074029.

5. Georgiopoulou, M., and Lyberatos, G. (2018). Life cycle assessment of the use of alternative fuels in cement kilns: A case study. J. Environ. Manage. *216*, 224–234. https://doi.org/10.1016/j.jenvman.2017.07.017.

6. Çankaya, S. (2020). Investigating the environmental impacts of alternative fuel usage in cement production: a life cycle approach. Environ. Dev. Sustain. *22*, 7495–7514. https://doi.org/10.1007/s10668-019-00533-y.

7. Chousidis, N., Rakanta, E., Ioannou, I., and Batis, G. (2015). Mechanical properties and durability performance of reinforced concrete containing fly ash. Constr. Build. Mater. *101*, 810–817. https://doi.org/10.1016/j.conbuildmat.2015.10.127.

8. Escalante-Garcıá, J.I., and Sharp, J.H. (2001). The microstructure and mechanical properties of blended cements hydrated at various temperatures. Cement Concr. Res. *31*, 695–702. https://doi.org/10.1016/S0008-8846(01)00471-9.

9. Mehta, A., and Ashish, D.K. (2020). Silica fume and waste glass in cement concrete production: A review. J. Build. Eng. *29*, 100888. https://doi.org/10.1016/j.jobe.2019.100888.

10. Provis, J.L. (2018). Alkali-activated materials. Cement Concr. Res. *114*, 40–48. https://doi.org/10.1016/j.cemconres.2017.02.009.

11. Miller, S.A. (2018). Supplementary cementitious materials to mitigate greenhouse gas emissions from concrete: can there be too much of a good thing? J. Clean. Prod. *178*, 587–598. https://doi.org/10.1016/j.jclepro.2018.01.008.

12. Fredricks, J.L., Iyer, H., McDonald, R., Hsu, J., Jimenez, A.M., and Roumeli, E. (2021). Spirulina-based composites for 3d-printing. J. Polym. Sci. *59*, 2878–2894. https://doi.org/10.1002/pol.20210683.

13. Duraj-Thatte, A.M., Manjula-Basavanna, A., Courchesne, N.-M.D., Cannici, G.I., Sánchez-Ferrer, A., Frank, B.P., van't Hag, L., Cotts, S.K., Fairbrother, D.H., Mezzenga, R., and Joshi, N.S. (2021). Water-processable, biodegradable and coatable aquaplastic from engineered biofilms. Nat. Chem. Biol. *17*, 732–738. https://doi.org/10.1038/s41589-021-00773-y.

14. Roumeli, E., Hendrickx, R., Bonanomi, L., Vashisth, A., Rinaldi, K., and Daraio, C. (2022). Biological matrix composites from cultured plant cells. Proc. Natl. Acad. Sci. USA *119*, e2119523119. https://doi.org/10.1073/pnas.2119523119.

15. Campbell, I.R., Lin, M.-Y., Iyer, H., Parker, M., Fredricks, J.L., Liao, K., Jimenez, A.M., Grandgeorge, P., and Roumeli, E. (2023). Progress in sustainable polymers from biological matter. Annu. Rev. Mater. Res. *53*, 81–104. https://doi.org/10.1146/annurev-matsci-080921-083655.

16. Iyer, H., Grandgeorge, P., Jimenez, A.M., Campbell, I.R., Parker, M., Holden, M., Venkatesh, M., Nelsen, M., Nguyen, B., and Roumeli, E. (2023). Fabricating strong and stiff bioplastics from whole spirulina cells. Adv. Funct. Mater. *33*, 2302067. https://doi.org/10.1002/adfm.202302067.

17. Chen, X., Matar, M.G., Beatty, D.N., and Srubar, W.V. (2021). Retardation of portland cement hydration with photosynthetic algal biomass. ACS Sustainable Chem. Eng. *9*, 13726–13734. https://doi.org/10.1021/acssuschemeng.1c04033.

18. Lin, M.-Y., Grandgeorge, P., Jimenez, A.M., Nguyen, B.H., and Roumeli, E. (2023). Long-term hindrance effects of algal biomatter on the hydration reactions of Ordinary Portland cement. ACS Sustain. Chem. Eng. *11*, 8242–8254. https://doi.org/10.1021/acssuschemeng.2c07539.

19. Acarturk, B.C., Jungclaus, M.A., Torres, M., Lash, B., and Srubar, W.V., III. (2024). Effect of algal biomass on the properties of calcium sulfoaluminate cement. ACS Sustain. Chem. Eng. *12*, 8690–8701. https://doi.org/10.1021/acssuschemeng.4c01007.

20. Srinivasan, C.B., Narasimhan, N.L., and Ilango, S.V. (2003). Development of rapid-set high-strength cement using statistical experimental design. Cement Concr. Res. *33*, 1287–1292. https://doi.org/10.1016/S0008-8846(03)00041-3.

21. Li, Y., Shen, L., Mirmoghtadaei, R., and Ai, L. (2017). A design of experiment approach to study the effects of raw material on the performance of geopolymer concrete. Adv. Civ. Eng. Mater. *6*, 526–549. https://doi.org/10.1520/ACEM20160007.

22. Li, Z., Yoon, J., Zhang, R., Rajabipour, F., Srubar III, W.V., Dabo, I., and Radlińska, A. (2022). Machine learning in concrete science: Applications, challenges, and best practices. npj Comput. Mater. *8*, 127. https://doi.org/10.1038/s41524-022-00810-x.

23. Ben Chaabene, W., Flah, M., and Nehdi, M.L. (2020). Machine learning prediction of mechanical properties of concrete: Critical review. Constr. Build. Mater. *260*, 119889. https://doi.org/10.1016/j.conbuildmat.2020.119889.

24. Li, Z., Pei, T., Ying, W., Srubar, W.V., III, Zhang, R., Yoon, J., Ye, H., Dabo, I., and Radlińska, A. (2024). Can domain knowledge benefit machine learning for concrete property prediction? J. Am. Ceram. Soc. *107*, 1582–1602. https://doi.org/10.1111/jace.19549.

25. Pfeiffer, O.P., Gong, K., Severson, K.A., Chen, J., Gregory, J.R., Ghosh, S., Goodwin, R.T., and Olivetti, E.A. (2024). Bayesian design of concrete with amortized gaussian processes and multi-objective optimization. Cement Concr. Res. *177*, 107406. https://doi.org/10.1016/j.cemconres.2023.107406.

26. Ament, S., Witte, A., Garg, N., and Kusuma, J. (2023). Sustainable concrete via bayesian optimization. Preprint at arXiv. https://doi.org/10.48550/arXiv.2310.18288.

27. Grandgeorge, P., Campbell, I.R., Nguyen, H., Brain, R., Parker, M., Edmundson, S., Rose, D., Homolke, K., Subban, C., and Roumeli, E. (2024). Adhesion in thermomechanically processed seaweed-lignocellulosic composite materials. MRS Bull. *49*, 787–801. https://doi.org/10.1557/s43577-024-00734-5.

28. Yeh, I.-C. Concrete Compressive Strength. UCI Machine Learning Repository (2007). doi: 10.24432/C5PK67.

29. Golovin, D., Solnik, B., Moitra, S., Kochanski, G., Karro, J., and Sculley, D. Google vizier: A service for black-box optimization. In: Proceedings of the 23rd ACM SIGKDD International Conference on Knowledge Discovery and Data Mining (2017):doi:10.1145/3097983.3098043.

30. Li, L., Jamieson, K., DeSalvo, G., Rostamizadeh, A., and Talwalkar, A. (2018). Hyperband: A novel bandit-based approach to hyperparameter optimization. J. Mach. Learn. Res. *18*, 1–52.

31. Dai, Z., Yu, H., Low, B. K. H., and Jaillet, P. 2019 (Bayesian optimization meets bayesian optimal stopping. In Proceedings of the 36th International Conference on Machine Learning (Proceedings of Machine Learning Research) 97: 1496–1506).

32. Belakaria, S., Doppa, J. R., Fusi, N., and Sheth, R. Bayesian optimization over iterative learners with structured responses: A budget-aware planning approach. In Proceedings of The 26th International Conference on Artificial Intelligence and Statistics (2023).

33. Young, B.A., Hall, A., Pilon, L., Gupta, P., and Sant, G. (2019). Can the compressive strength of concrete be estimated from knowledge of the mixture proportions?: New insights from statistical analysis and machine learning methods. Cement Concr. Res. *115*, 379–388. https://doi.org/10.1016/j.cemconres.2018.09.006.

34. C150, A. Standard specification for portland cement. Tech. Rep. ASTM Internation West Conshohocken, PA (2021). https://doi.org/10.1520/C0150-07.

35. Jennings, H.M. (2000). A model for the microstructure of calcium silicate hydrate in cement paste. Cement Concr. Res. *30*, 101–116. https://doi.org/10.1016/S0008-8846(99)00209-4.

36. Feiz, R., Ammenberg, J., Baas, L., Eklund, M., Helgstrand, A., and Marshall, R. (2015). Improving the CO2 performance of cement, part i: utilizing life-cycle assessment and key performance indicators to assess development within the cement industry. J. Clean. Prod. *98*, 272–281. https://doi.org/10.1016/j.jclepro.2014.01.083.

37. Bond, F.C. (1961). Crushing and grinding calculations, Part I. Br. Chem. Eng. *6*, 378–385.

38. Pane, I., and Hansen, W. (2005). Investigation of blended cement hydration by isothermal calorimetry and thermal analysis. Cement Concr. Res. *35*, 1155–1164. https://doi.org/10.1016/j.cemconres.2004.10.027.

39. Ge, X., Goodwin, R. T., Yu, H., Romero, P., Abdelrahman, O., Sudhalkar, A., Kusuma, J., Cialdella, R., Garg, N., and Varshney, L. R. Accelerated design and deployment of low-carbon concrete for data centers. In: Proceedings of the 5th ACM SIGCAS/SIGCHI Conference on Computing and Sustainable Societies (2022). https://doi.org/10.48550/arXiv.2204.05397.

40. C1074, A. Standard practice for estimating concrete strength by the maturity method. Tech. Rep. ASTM Internation West Conshohocken, PA (2019). https://doi.org/10.1520/C1074-17.

41. C94, A. (2024). Standard specification for ready-mixed concrete. In Tech. Rep. ASTM Internation West Conshohocken, PA. https://doi.org/10.1520/C0094_C0094M-23.

42. Committee 214, A. Guide to evaluation of strength test results of concrete. Tech. Rep. American Concrete Institute Farmington Hills, MI (2011).

43. Crawford, R.H., Bontinck, P.-A., Stephan, A., Wiedmann, T., and Yu, M. (2018). Hybrid life cycle inventory methods – a review. J. Clean. Prod. *172*, 1273–1288. https://doi.org/10.1016/j.jclepro.2017.10.176.

44. C109, A. Standard test method for compressive strength of hydraulic cement mortars (using 2-in. or [50 mm] cube specimens). Tech. Rep. ASTM Internation West Conshohocken, PA (2021). https://doi.org/10.1520/C0109_C0109M-20.

45. Ali, M.B., Saidur, R., and Hossain, M.S. (2011). A review on emission analysis in cement industries. Renew. Sustain. Energy Rev. *15*, 2252–2261. https://doi.org/10.1016/j.rser.2011.02.014.

46. Duarte, C.M. (1992). Nutrient concentration of aquatic plants: Patterns across species. Limnol. Oceanogr. *37*, 882–889. https://doi.org/10.4319/lo.1992.37.4.0882.

47. Tzachor, A., Smidt-Jensen, A., Ramel, A., and Geirsdóttir, M. (2022). Environmental impacts of large-scale spirulina (Arthrospira platensis) production in Hellisheidi geothermal park Iceland: Life cycle assessment. Mar. Biotechnol. *24*, 991–1001. https://doi.org/10.1007/s10126-022-10162-8.

48. Koesling, M., Kvadsheim, N.P., Halfdanarson, J., Emblemsvåg, J., and Rebours, C. (2021). Environmental impacts of protein-production from farmed seaweed: Comparison of possible scenarios in norway. J. Clean. Prod. *307*, 127301. https://doi.org/10.1016/j.jclepro.2021.127301.

49. Ngamnikom, P., and Songsermpong, S. (2011). The effects of freeze, dry, and wet grinding processes on rice flour properties and their energy consumption. J. Food Eng. *104*, 632–638. https://doi.org/10.1016/j.jfoodeng.2011.02.001.

50. Schneider, C.A., Rasband, W.S., and Eliceiri, K.W. (2012). NIH Image to ImageJ: 25 years of image analysis. Nat. Methods *9*, 671–675. https://doi.org/10.1038/nmeth.2089.

51. Williams, C.K., and Rasmussen, C.E. (2006). Gaussian Processes for Machine Learning, *2* (MIT Press Cambridge).

52. Greenhill, S., Rana, S., Gupta, S., Vellanki, P., and Venkatesh, S. (2020). Bayesian optimization for adaptive experimental design: A review. IEEE Access *8*, 13937–13948. https://doi.org/10.1109/ACCESS.2020.2966228.

53. Gelbart, M. A., Snoek, J., and Adams, R. P. Bayesian optimization with unknown constraints. In: 30th Conference on Uncertainty in Artificial Intelligence, UAI 2014 (2014). https://doi.org/10.48550/arXiv.1403.5607.

54. Hernandez-Lobato, J. M., Gelbart, M., Hoffman, M., Adams, R., and Ghahramani, Z. Predictive entropy search for bayesian optimization with unknown constraints. In: Proceedings of the 32nd International Conference on Machine Learning (2015): 1699–1707.

Matter, Volume *8*

Supplemental information

Closed-loop optimization using machine learning for the accelerated design of sustainable cements incorporating algal biomatter

Meng-Yen Lin, Kristen Severson, Paul Grandgeorge, and Eleftheria Roumeli

Supplemental Figures

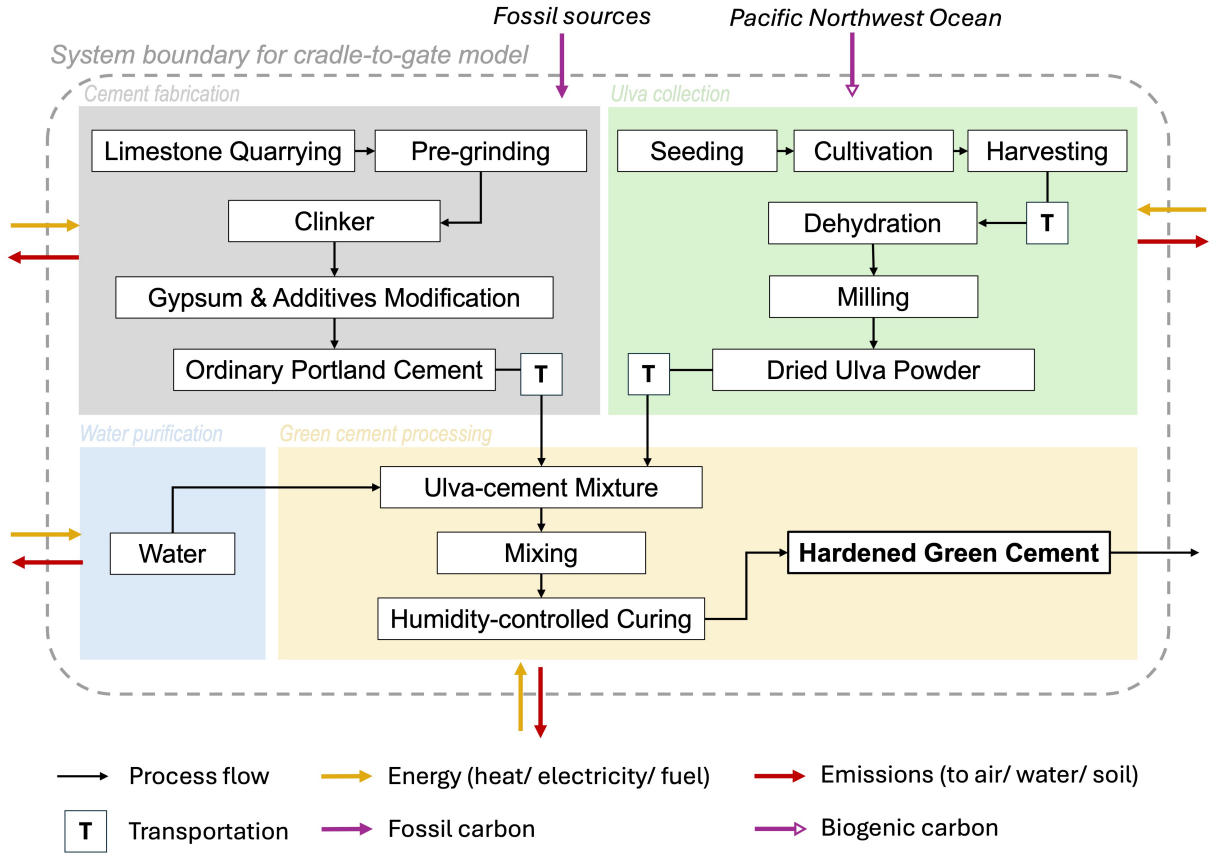

Figure S1: **Cradle-to-gate process flow for the life cycle of *Ulva*-cement.** The supply chain of ordinary Portland cement is established based on [S1], and the cultivation of sugar kelp [S2] is used as a proxy data for *Ulva*.

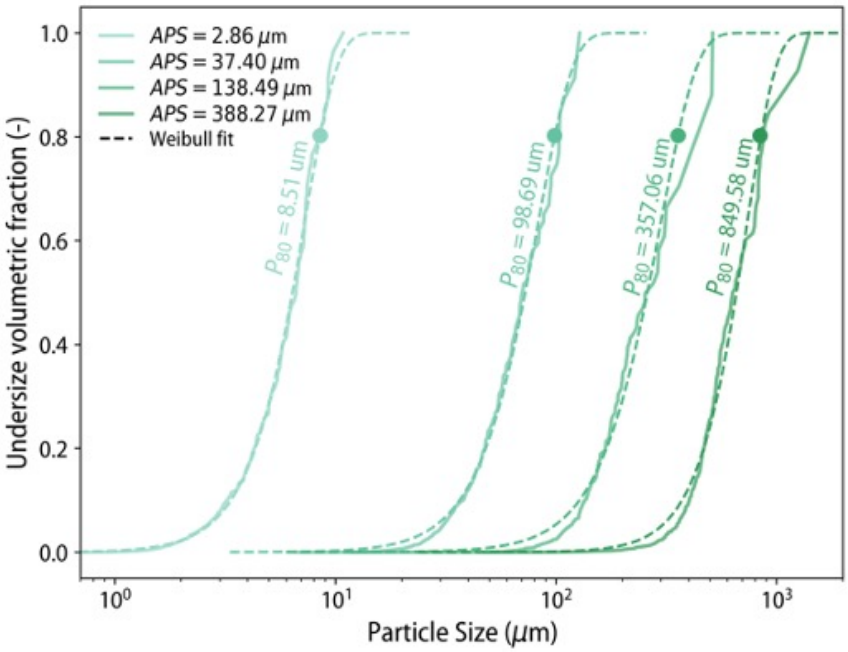

Figure S2: **Particle size distribution of the four different *Ulva* powders used in this study.** The cumulative particle undersize was fitted using a Weibull distribution (of the form $1 - \exp(-PS/\lambda)^n$. The average particle size (APS) is provided in the legend and the the 80% passing size ($P80$, based on the fitted Weibull distribution), is provided next to the corresponding curves.

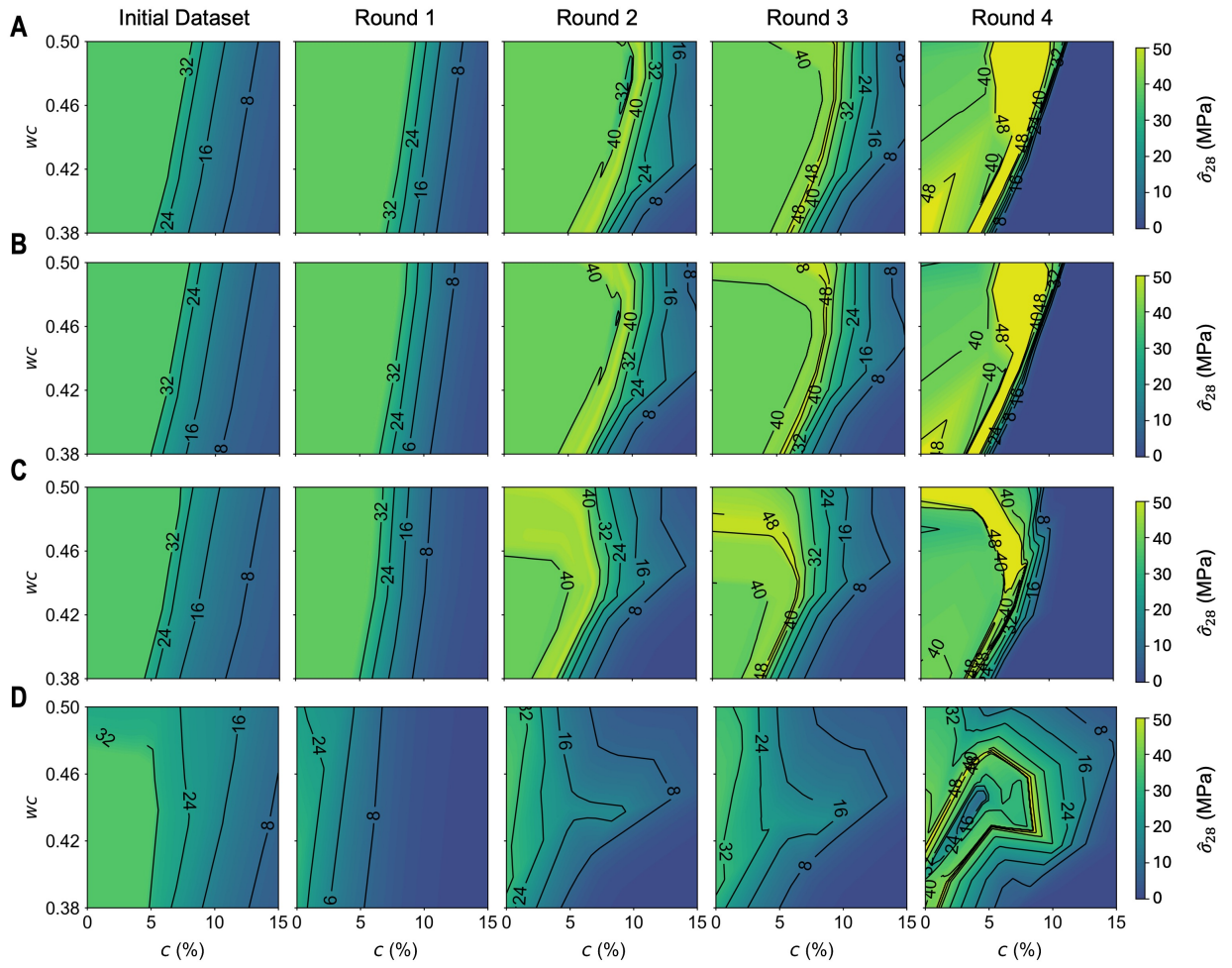

Figure S3: **Model evolution of different** *APS* **during the closed-loop iteration.** Contour plots indicate the predicted compressive 28-day strength $\hat{\sigma}$ as a function of water-cement ratio *wc* and *Ulva* concentration *c* over the rounds of experimentation. All plots show data at 95% *RH*. Rows (A), (B), (C), and (D) correspond to *APS* 2.86, 37.40, 138.49, and 388.27 μm, respectively. Particularly in round 4, these plots visualize that higher compressive strengths are achievable for high concentrations for lower *APS* (rows (A) and (B)).

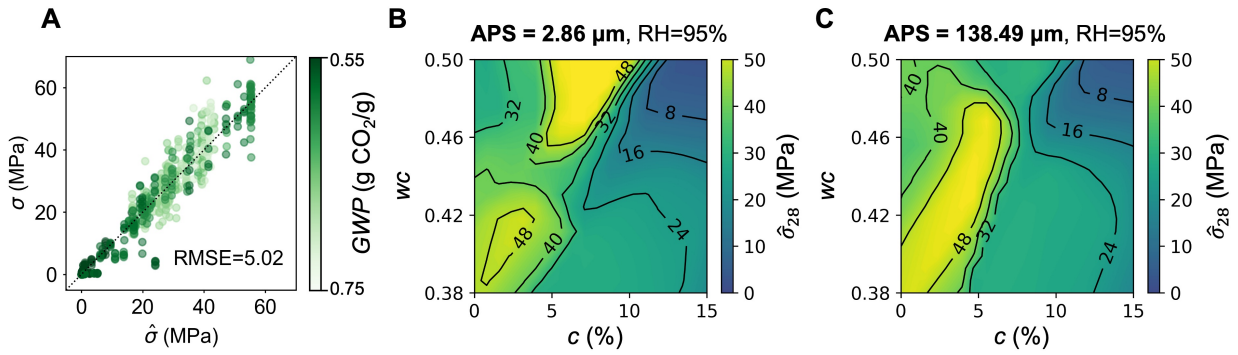

Figure S4: **Predicted results from full data model.** (A) The model performance of the predictive model using full data model, comparing the estimated compressive strength $\hat{\sigma}$ and measured compressive strength σ at different time points. Contour plots of the predicted compressive 28-day strength $\hat{\sigma}$ as a function of water-cement ratio wc and *Ulva* concentration c for $APS = 2.86\mu m$ (B) and $APS = 138.49\mu m$ (C) at 95% RH. We observe that as APS increases, the valley disappears at around $c = 5\%$ and $wc = 0.45$, which we ascribe to the lack of data points under certain conditions.

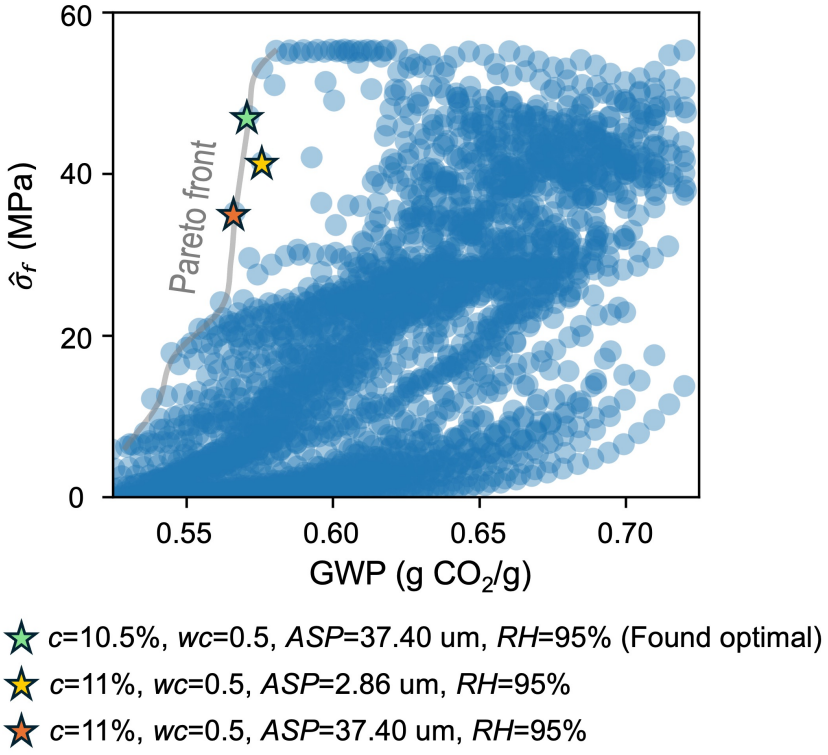

Figure S5: **Trade-off of strength and GWP for formulations near the Pareto front.** The found optimal formulation and another comparable formulation $c = 11\%$, $wc = 0.5$, $APS = 37.40\mu m$, $RH = 95\%$ (not predicted qualified during closed-loop optimization) are on the Pareto front. In addition, due to reducing particle size with increasing milling energy, $c = 11\%$, $wc = 0.5$, $APS = 2.86\mu m$, $RH = 95\%$ is not on the Pareto front.

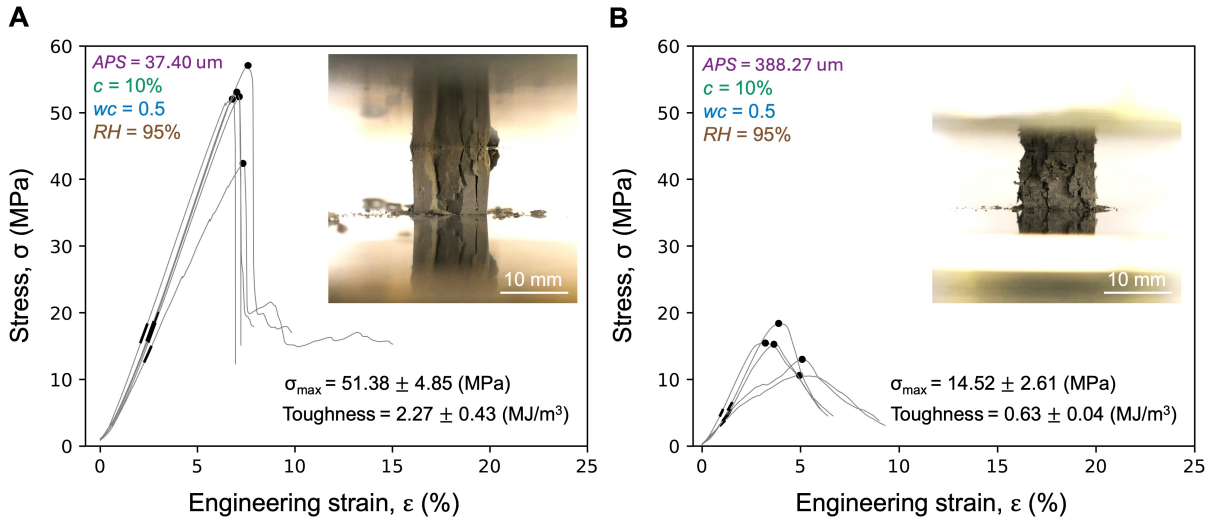

Figure S6: **Fracture behavior and compressive stress-strain curves of green cement with different *Ulva* particle sizes on day 28.** (A) Samples of $APS = 37.40\mu m$, $c = 10\%$, $wc = 0.5$, and $RH = 95\%$ show classic semi-brittle failure with drastic strength reduction and instant crack development upon fracture. (B) Samples of $APS = 388.27\mu m$, $c = 10\%$, $wc = 0.5$, and $RH = 95\%$ present more plastic deformation after the ultimate compressive strength and the jagged crack pattern keeps developing with deformation.

Supplemental Tables

Table S1: Recommended formulations for optimization iteration. Table S1 lists the experiments during closed loop testing, the duration of the experiment, whether or not our approach determined the formulation was qualifying, the observed 28-day compressive strength and the GWP. We note that one formulation from week 4 was incorrectly labeled non-qualifying; this incorrect point also happens to be the true optimum.

Although the entire design space was not measured, we are confident in our assessment of the optimal point, wc=0.5, c=11%, APS=37.40μm, and RH=95%. To improve upon this point, a formulation must have one (or more) of these characteristics: higher water-to-cement ratio, higher biomass concentration, higher average particle size distribution, relative humidity of 50 (very low impact comparatively) and meet the strength criterion. Considering the results in Table S1 along with the results in Table S4, which were performed to further investigate the design space, we observe that formulations which would have lower GWP, all are non-qualifying. Increasing biomass (experiment 3 of week 4), increasing particle size while decreasing biomass (experiment 4 of the additional experiments), and decreasing particle size while increasing biomass (experiment 2 of week 4) all result in non-qualifying formulations. Noting that 0.5 is the maximum wc, there are effectively no untested formulations which could improve upon the stated optimum.

	c (%)	wc	$APS(\mu m)$	RH (%)	Experiment Duration (Days)	Qualifying Formulation	Observed Avg. 28-Day Strength (MPa)	GWP (g CO_2/g)
Week 1	7.5	0.5	37.40	95%	4	✓	51.8	0.599
	8	0.5	2.86	95%	4	✓	54.5	0.601
	7	0.5	37.40	95%	2	✓	54.7	0.604
	7	0.5	138.49	95%	7		28.8	0.603
Week 2	8.5	0.5	37.40	95%	2	✓	54.5	0.590
	9	0.5	2.86	95%	2	✓	58.7	0.593
	8	0.5	37.40	95%	2	✓	54.7	0.595
	8.5	0.5	2.86	95%	2	✓	53.9	0.597
Week 3	11	0.5	2.86	95%	4	✓	40.5	0.576
	10	0.5	37.40	95%	2	✓	51.4	0.576
	10.5	0.5	37.40	95%	2	✓	47.4	0.571
	10.5	0.5	2.86	95%	4	✓	51.9	0.580
Week 4	11	0.5	37.40	95%	2		35.7	0.567
	12	0.5	2.86	95%	2		17.5	0.567
	11.5	0.5	37.40	95%	2		3.7	0.562
	11.5	0.48	37.40	95%	2		6.5	0.569

Table S2: Peak analysis of XRD patterns for samples with different *Ulva* particle sizes. Peak analysis is based on Figure 6C. The *Ulva*-cements are made at fixed $c = 10\%$, $wc = 0.5$, and $RH = 95\%$.

	Peak Location (2θ)	Peak Intensity (a.u.)		Peak Width (°)		Crystallite Size (nm)	
$ASP(\mu m)$		388.27	37.40	388.27	37.40	388.27	37.40
Ettringite	15.93	0.74	0.96	0.61	0.41	14.53	21.80
Portlandite	18.18	2.20	1.21	0.61	0.61	14.57	14.58
Calcite	23.09	1.19	1.33	0.61	0.41	14.69	22.03
Calcite	29.44	3.03	3.15	0.61	0.61	14.88	14.88
Alite/ Belite	32.30	1.94	2.66	1.02	0.82	8.99	11.24
Portlandite	34.14	4.41	3.20	0.82	1.02	11.29	9.03
Alite/ Belite	41.30	0.99	1.10	1.20	1.02	9.22	9.23
Portlandite	47.23	1.95	1.63	0.61	0.82	15.70	11.78
Portlandite	50.92	1.51	1.35	0.61	0.61	15.93	15.94

Table S3: Additional experimentation tested at all time points in full data model.

c (%)	wc	$APS(\mu m)$	RH (%)	Observed Avg. 28-Day Strength (MPa)
5	0.5	388.27	95	24.4
5	0.5	138.49	95	35.3
10	0.5	388.27	95	14.5
10	0.5	138.49	95	28.0

Table S4: Initial experimentation based on Latin Hypercube design.

c (%)	wc	$APS(\mu m)$	RH (%)	Observed Avg. 28-Day Strength (MPa)
0.5	0.42	37.40	50	41.5
0.5	0.42	388.27	10	28.1
0.5	0.44	2.86	95	40.0
0.5	0.46	388.27	10	24.0
0.5	0.48	37.40	95	37.5
0.5	0.48	388.27	50	33.3
1	0.38	138.49	10	42.0
1	0.4	37.40	50	48.7
1	0.44	138.49	50	36.0
1	0.46	388.27	50	31.9
1	0.48	388.27	50	29.8
1	0.5	2.86	50	33.0
5	0.38	138.49	95	27.8
5	0.4	138.49	95	46.9
5	0.42	2.86	95	45.6
5	0.44	37.40	10	43.7
5	0.5	2.86	95	48.7
5	0.5	2.86	10	31.7
15	0.38	138.49	10	0
15	0.4	37.40	10	0.7
15	0.4	138.49	10	0
15	0.44	37.40	95	16.8
15	0.46	388.27	95	6.7
15	0.5	2.86	50	3.1

Supplemental Note S1

Measurement of CO_2 Emissions from Biomass Degradation during Curing

To assess the possible CO_2 emissions from any possible degradation reactions of components within Ulva during cement curing reactions, where the high alkalinity may provide grounds for such degradation pathways we devised the following experiment. We followed a similar method to ASTM D5988 [S3], which measures the degradation and CO_2 emission during the aerobic biodegradation of plastic materials through reactions of emitted CO_2 with potassium hydroxide (KOH). The CO_2 capturing reaction of KOH is:

$$2KOH + CO_2 \rightarrow H_2O + K_2CO_3 \tag{1}$$

To prevent the cement hydration reaction from affecting the measurement of CO_2 emission resulting from the *Ulva* degradation, we first prepared the cement alkaline solution at pH 13.3 by extracting the supernatant of the cement slurry at w/c 0.6 through centrifugation to simulate the alkaline environment in cement. Next, we submerge 3 g of *Ulva* powder in 30 mL of cement alkaline solution. Next to the *Ulva* sample submerging in the alkaline solution, we place another beaker of 20 mL 0.5 M KOH. Both beakers are placed in a sealed desiccator for 8 days, as shown in Figure S7A, while blank desiccators only containing the KOH solution are prepared as controls to account for ambient activity. Note that this test is done in triplicates and the test duration of 8 days is chosen because the pore water in cement would substantially decrease over 7 days.

To assess the amount of emitted CO_2 when *Ulva* is subject to a cement alkaline environment we need to measure the amount of consumed KOH during CO_2-capturing reactions, which is achieved through titration with hydrochloride (HCl) according to the following reaction:

$$HCl + KOH \rightarrow H_2O + KCl \tag{2}$$

Given the initial concentration of KOH, $c_{KOH,i}$, of 0.5 M, the amount of KOH consumed during the curing process can be estimated. First, using titration reaction Equation 2, we obtain the required neutralization volume of HCl, V_{HCl}, to reach pH 7.0. The titration curves are shown in Figure S7B. Next, we can calculate the concentration of KOH solution at the time of measurement, $c_{KOH,t}$, by Equation 3:

$$c_{KOH,t} \cdot V_{KOH} = c_{HCl} \cdot V_{HCl} \tag{3}$$

where c_{HCl}, the concentration of HCl, is 0.25 M, and the amount of KOH solution, V_{KOH}, is 20 mL. By comparing the difference in KOH concentrations between the initial 0.5 M and $c_{KOH,t}$, we can get the moles of CO_2, n_{CO_2}, absorbed by KOH over time using the 1/2 molar ratio of CO_2 and KOH in Equation 1.

$$n_{CO_2}(mole) = \frac{1}{2}(c_{KOH,i} - c_{KOH,t})(mole/L) \cdot V_{KOH}(L) \tag{4}$$

The amount of CO_2 in grams, W_{CO_2}, consumed by KOH over time is:

$$W_{CO_2}(g) = 44(g/mole) \cdot n_{CO_2}(mole) \tag{5}$$

The concentrations of KOH in the controls and samples on day 8 are shown in Figure S7C. We find the differences in KOH concentrations between the controls and *Ulva* samples are not statistically significant, as indicated by Welch's t-test (p=0.13). This result suggests that when *Ulva* are subjected to the cement alkaline environment, the CO_2 emissions, in the first 8 days are negligible. It is important to note that this experiment simulates *Ulva*'s reaction to an abundant cement alkaline solution and does not represent actual CO_2 emissions in *Ulva*-cement composites, where the ratio of *Ulva* to alkaline solutions would be much lower - likely resulting in an even lower GWP contribution from *Ulva* degradation. Moreover, this result does not account for long-term (e.g., 100-year) CO_2 emissions, as potential microbial interactions beyond our LCA boundaries could alter the outcome.

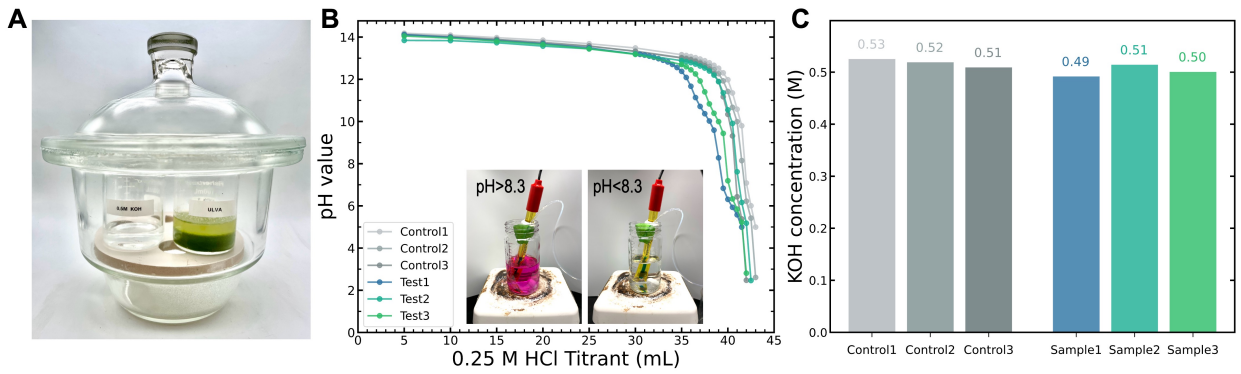

Figure S7: **Experiments for CO_2 emissions simulating *Ulva* degradation in green cements** (A) A sealed glass desiccator containing two beakers. One with KOH solution and the other with *Ulva* in a cement alkaline solution. (B) Titration curves of KOH solutions using 0.25 N HCl. The inset images show the color change of the solution with the addition of 100 μm phenolphthalein when pH decreases from basic to acidic. (C) Concentrations of KOH solutions at day 8.

Supplemental Note S2

Comparison of Simulation Data

To develop a simulator for the methodological comparison, we consider three models, amortized Gaussian processes (the model class used in the closed-loop design), Gaussian process with Matérn kernel, and Gaussian process with a product kernel. Note these are the same model types used for the comparison in the "comparing different experiment design strategies" section and they are explained in additional detail in the "comparison methodology" section. Using the *full data* dataset (as described in Table S1-S4), the three models are trained using the same train/test split. Models are compared based on the root mean square error (RMSE) for all time points as well as 28 days only; results are reported in Table S5. Although both GP models with Matérn and product kernels have lower RMSE during training, they generalize poorly, as indicated by test performance, compared to the aGP model. This observation is true for all time points and the subset of 28-day time points. Therefore we proceed with the aGP model as the best available simulator. Note that the metrics for the aGP do not exactly match those reported in Figure 5 as the metrics presented in this section are calculated using all available data as opposed to only the closed-loop and initial datasets. The difference is the validation experiments (listed in Table S3). The models (referred to in the text as *full data model*) are identical, but evaluated differently in the different contexts.

Table S5: Metrics comparing various *full data* models.

	aGP		GP-Matern		GP-Product	
	Train	Test	Train	Test	Train	Test
RMSE (MPa), all time points	4.39	6.41	3.81	11.00	3.91	11.81
RMSE (MPa), 28 days only	5.38	8.90	4.91	12.70	5.07	15.06

Supplemental references

[S1] Ali, M.B., Saidur, R., and Hossain, M.S. (2011). A review on emission analysis in cement industries. *Renewable and Sustainable Energy Reviews*, **15**, 2252–2261. doi: 10.1016/j.rser.2011.02.014.

[S2] Koesling, M., Kvadsheim, N.P., Halfdanarson, J., Emblemsvåg, J., and Rebours, C. (2021). Environmental impacts of protein production from farmed seaweed: Comparison of possible scenarios in Norway. *Journal of Cleaner Production*, **307**, 127301. doi: 10.1016/j.jclepro.2021.127301.

[S3] ASTM D5988. (2018). Standard test method for determining aerobic biodegradation of plastic materials in soil. *ASTM International*, West Conshohocken, PA. doi: 10.1520/D5988-18.